THESIS

AN INVESTIGATION OF AMMONIA AND INORGANIC PARTICULATE MATTER IN CALIFORNIA DURING THE CALNEX CAMPAIGN

Submitted by

Luke D. Schiferl

Department of Atmospheric Science

In partial fulfillment of the requirements

For the Degree of Master of Science

Colorado State University

Fort Collins, Colorado

Fall 2012

Master's Committee:

Advisor: Colette L. Heald

Jeffrey L. Collett, Jr.
Jay M. Ham

ABSTRACT

AN INVESTIGATION OF AMMONIA AND INORGANIC PARTICULATE MATTER IN CALIFORNIA DURING THE CALNEX CAMPAIGN

Over the last century, the rise of industrial agriculture has greatly increased the emission of ammonia (NH_3) from livestock waste and synthetic crop fertilizers to the atmosphere. Ammonium (NH_4^+) aerosol, which can be formed through the neutralization of atmospheric acids by NH_3, is a key component of particulate matter (PM) in the atmosphere. PM causes negative human health effects and reduces visibility, and transport and deposition of excess NH_3 can cause environmental degradation.

Airborne observations of gas precursors and inorganic aerosol taken during the CalNex campaign in May and June 2010 are used in this study to investigate the role of NH_3 in PM formation in California and test the representation of the key processes relevant to this chemical system in the GEOS-Chem chemical transport model.

Evaluation of the 0.5° x 0.667° horizontal resolution nested model with observations shows a large underestimation (5.4 ppb median bias in the lowest 1 km) of NH_3 in the Central Valley. This NH_3 underestimation is lower in the area surrounding Los Angeles (LA), only 1.4 ppb. Sulfur dioxide (SO_2) is also underestimated in both regions, while nitric acid (HNO_3) shows little bias. Near-surface simulated inorganic PM is under-predicted by 1.28 μg sm^{-3} in the LA region and over-predicted in the Valley by 0.27 μg sm^{-3}.

Investigation of model sensitivity to the processes of gas-particle partitioning, wet deposition, dry deposition and emissions reveal that emissions have the largest potential for correction of model deficiencies. Increases to anthropogenic livestock NH_3 emissions by a factor

of 5 and anthropogenic SO_2 emissions in the Valley by factors from 3 - 10 eliminates the bias in the simulation of gases in both regions and PM near LA, where under-prediction of nitrate (NO_3^-) is reduced from 0.64 μg sm^{-3} to 0.12 μg sm^{-3} in the lowest 1 km. An increase in NH_3 emissions in the LA region is critical to capturing ammonium nitrate (NH_4NO_3) formation down-wind of the city core.

Using this modified emissions simulation, seasonal PM differences in the two regions and the export of excess NH_3 out of the Valley are explored. Mean June simulated PM concentration in the lowest 1 km is 3.48 μg sm^{-3} near LA (38% NO_3^- and 39% SO_4^{2-}, by mass) and 1.98 μg sm^{-3} in the Valley (44% NO_3^- and 32% SO_4^{2-}, by mass). These simulated PM concentrations are 2 times greater in the Valley in December than in June, when NH_4NO_3 formation is favored by colder temperatures. However, LA simulated PM concentration falls by 53% in December compared to June, likely due to lower winter NH_3 emissions. Both the model and IASI satellite observations indicate that large amounts of excess NH_3 are transported from the Valley to southeastern California in the summertime which may negatively affect ecosystems in this area.

ACKNOWLEDGMENTS

I would like to thank the following, who were vital in the completion of this project:

- Colette Heald, my advisor, for unfailing guidance and support.
- My committee members, Jeff Collett and Jay Ham, for their questions, suggestions and expertise.
- Other members of the Heald Group, Bonne Ford Hotmann, Ashley Berg, Maria Val Martin, Dave Ridley, Kateryna Lapina and Leigh Munchak, for analysis advice and feedback, coding assistance and social interaction.
- Stu McKeen for NEI-2005 sector separation and Aaron van Donkelaar for emissions gridding.
- Christine Wiedinmyer for the FINN emissions product and Jingqiu Mao for implementation of FINN into GEOS-Chem.
- John Nowak, John Holloway, Andy Neuman, Roya Bahreini and Ann Middlebook at NOAA/ESRL for the CalNex aircraft observations.
- GEOS-Chem support staff and community for model documentation and issue resolution.
- The Environmental Protection Agency and National Park Service for funding.

TABLE OF CONTENTS

1. Introduction

1.1 Ammonia and Atmospheric Nitrogen

Ammonia (NH_3) is emitted to the atmosphere from many anthropogenic as well as natural sources. Prior to the implementation of industrial agriculture practices, the largest sources of ammonia on land were combustion associated with wildfires and domestic fuel burning. Today, large agriculture operations account for the majority of global ammonia emissions [*Dentener and Crutzen*, 1994]. These emission sources include fertilizers applied to plant crops and the waste by-products of domesticated animals, particularly those raised in large feedlots. Other sources of ammonia include industrial manufacturing processes, soil, the ocean, fossil fuel combustion and automobile catalytic conversion [*Bouwman et al.*, 1997].

Human population growth, especially over the last century, has increased the need for reliable food sources in the form of crops and livestock. Plants require fixed nitrogen in order to support the process of photosynthesis, which provides energy to propagate all life processes, including the conversion of carbon dioxide (CO_2) from the air into leaves, stems and roots. Fixed nitrogen refers to the nitrogen in compounds such as ammonia, nitrates and nitrites, which is in physically useful forms to plants, as opposed to the vast majority of the nitrogen pool which is inert triple-bonded atmospheric nitrogen (N_2). Prior to industrialization, the largest source of fixed nitrogen for plant growth was NO_x from lightning [*Vitousek*, 1994], which is able to break the triple bonds of N_2. While studies suggest a potential increase in lightning NO_x production with climate change [*Schumann and Huntrieser*, 2007], the trend is small compared to the increases in anthropogenic fixation of ammonia through the Haber-Bosch process over the last century [*Erisman et al.*, 2008; *Sutton et al.*, 2008]. This increase in fixed nitrogen has modified the nitrogen balance in many ecosystems.

Ammonia, from sources such as excess plant fertilizer and volatilized animal waste, can react with other constituent gases of the atmosphere. The reaction of ammonia with sulfuric and nitric acids can produce aerosol in the form of ammonium sulfate and ammonium nitrate (see Section 1.2). As a constituent of atmospheric particulate matter (PM), understanding the formation of these aerosols is important for understanding air quality and visibility issues, especially in high emission areas. These aerosols also have impacts on climate, given their ability to adjust the energy budget of the planet through scattering of solar radiation [*IPCC*, 2007]. Finally, the nitrogen contained in these aerosols can be transported and eventually deposited downwind. Ammonium compounds deposited on land can be used by plants as above; however, if oversaturated in the soil or aquatic ecosystems, environmental degradation through acidification and eutrophication may occur [*Erisman et al.*, 2007].

1.2 NH_x in the Atmosphere

Chemical reactions are an important loss mechanism of gaseous ammonia from the atmosphere. The formation of ammonium salts in the atmosphere is a coupled chemical and thermodynamic process, which is described briefly below (Source: [*Seinfeld and Pandis*, 2006]).

When dissolved in water (H_2O), which occurs in clouds and aqueous aerosols in the atmosphere, NH_3 equilibrates with ammonium ion (NH_4^+) and hydroxide ion (OH^-) (R1, R2). The production of hydroxide ions through this equilibrium indicates that ammonia is a base. In fact, ammonia is the most abundant basic gas in the atmosphere. Using the Henry's law coefficient for ammonia and the partitioning constants for the reactions, it is found that nearly all dissolved ammonia is in the form of ammonium ion under atmospheric conditions. Additionally, when droplet pH is lower than 5, almost all available ammonia will be dissolved into the aqueous

phase. The dissolution of ammonia into the aqueous phase is highly pH dependent, with the fraction of dissolved available ammonia dropping to 10 % in a neutral water droplet, given cloud liquid water content of 0.01 g m^{-3}.

$$NH_{3(g)} + H_2O \leftrightarrow NH_3 \cdot H_2O \quad \text{R1}$$

$$NH_3 \cdot H_2O \leftrightarrow NH_4^+{}_{(aq)} + OH^-{}_{(aq)} \quad \text{R2}$$

As a base, ammonia can react to neutralize atmospheric acids such as sulfuric acid (H_2SO_4). The products of dissolved NH_3 and H_2SO_4 in the aerosol can vary based on relative humidity (RH) and total available ammonia. In low RH conditions the lack of water results in transition into the solid aerosol phase as a progression of salt formation occurs with increasing total ammonia levels: ammonium bisulfate (NH_4HSO_4) to letovicite ($(NH_4)_3H(SO_4)_2$) to ammonium sulfate ($(NH_4)_2SO_4$). In higher RH conditions and at low total ammonia levels, the aerosol is more likely to stay in aqueous phase as a solution of H_2SO_4, sulfate (SO_4^{2-}) and NH_4^+, as NH_4HSO_4 and $(NH_4)_3H(SO_4)_2$ deliquesce at 40 % and 69 % RH, respectively, at 25˚C. When a high enough total ammonia level is reached, solid $(NH_4)_2SO_4$ is directly formed in the aerosol, associated with its higher deliquescence RH (DRH) of 80 %. R3 represents an overall equation for these reactions, as two NH_4^+ are required to neutralize one SO_4^{2-}.

$$2\ NH_{3(g)} + H_2SO_{4(aq)} \rightarrow (NH_4)_2SO_{4(aq,s)} \quad \text{R3}$$

After all available sulfuric acid has been neutralized, any remaining ammonia can react with nitric acid (HNO_3) to form ammonium nitrate (NH_4NO_3) aerosol (R4, R5). Thus, ammonium nitrate formation generally occurs in areas of high ammonia and nitric acid and low sulfate concentrations. When on the stable branch of the hygroscopic hysteresis curve, the phase of this ammonium nitrate aerosol is determined by comparing the DRH, itself determined by

temperature in R6 with the ambient RH. At 25 ˚C the DRH is 62 %, and increases to 77 % at 0˚C. When the DRH is greater (less) than the ambient RH, then the aerosol is in the solid (aqueous) phase, as in R4 (R5). If on the metastable branch of the hysteresis curve, the transition from aqueous to solid phase takes place at the efflorescence relative humidity (ERH). The ERH for NH_4NO_3 is much lower than the DRH as well as typical ambient relative humidities, ranging from 10 % to 30 % depending on the presence of SO_4^{2-}. Pure NH_4NO_3 is not observed to crystallize even close to 0 % RH.

$$NH_{3(g)} + HNO_{3(g)} \leftrightarrow NH_4NO_{3(s)} \quad \text{R4}$$

$$NH_{3(g)} + HNO_{3(g)} \leftrightarrow NH_4^+{}_{(aq)} + NO_3^-{}_{(aq)} \quad \text{R5}$$

$$\ln (DRH) = \frac{723.7}{T} + 1.6954 \quad \text{R6}$$

For solid NH_4NO_3 aerosol, the equilibrium of R4 is determined by a dissociation constant (K_p, R7), which increases with temperature and is quite sensitive, varying by two orders of magnitude over ambient conditions. Lower temperatures result in a lower dissociation constant and move the equilibrium of R4 toward the solid aerosol phase. However when the NH_4NO_3 aerosol is in the aqueous phase, the dissociation constant for R5 (K_{p2}, R8) depends on both RH and temperature. As the equilibrium constant (K_{AN}, R9) in the denominator of R8 decreases with temperature, increasing temperature increases K_{p2} and favors the gas phase. At constant temperature, the numerator of R8 depends on the activity of the species in this highly concentrated, nonideal solution. The activity is a product of the activity coefficient (γ), determined by involved thermodynamic calculations, and molality (m) of each species. An increase of RH decreases m and K_{p2} and shifts the equilibrium toward the aerosol phase as more NH_4NO_3 can be dissolved into the wetter aerosol. Ambient variations of RH and temperature can

change K_{p2} by several orders of magnitude. In the presence of ammonium sulfate, the ammonium sulfate ionic strength (Y, R10) also affects the equilibrium of R5.

$$\ln K_p = 84.6 - \frac{24220}{T} - 6.1 \ln\left(\frac{T}{298}\right) \qquad \text{R7}$$

$$K_{p2} = \frac{\gamma_{NH_4^+}\gamma_{NO_3^-} m_{NH_4^+} m_{NO_3^-}}{K_{AN}} \qquad \text{R8}$$

$$K_{AN} = 4 \times 10^{17} \exp\left\{64.7\left(\frac{298}{T} - 1\right) + 11.51\left[1 + \ln\left(\frac{298}{T}\right) - \frac{298}{T}\right]\right\} \qquad \text{R9}$$

$$Y = \frac{[NH_4NO_3]}{[NH_4NO_3]+3[(NH_4)_2SO_4]} \qquad \text{R10}$$

The addition of ammonium sulfate decreases Y and makes the aqueous solution more likely to shift toward the aqueous aerosol phase. Figure 1.1 shows the relationship between K_{p2}, RH and Y at constant temperature on both the stable and metastable branches, where K_{p2} =

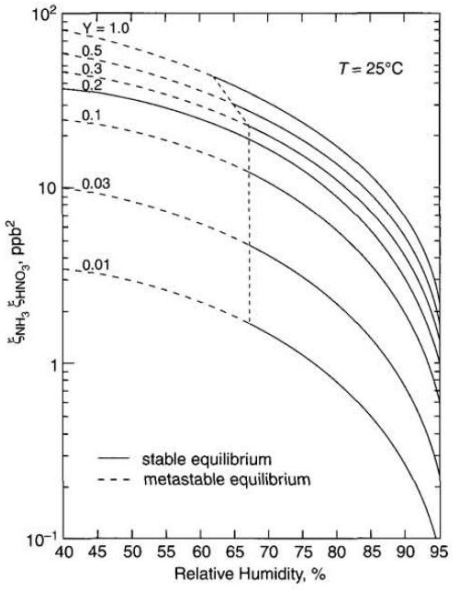

Figure 1.1: NH_4NO_3 equilibrium dissociation constant for a mixed solution of ammonium sulfate and ammonium nitrate at 298 K [*Seinfeld and Pandis*, 2006].

$\xi_{NH_3}\xi_{HNO_3}$. These multiple determining conditions of equilibrium as well as their high degree of variability in the atmosphere make measurement of ammonium nitrate difficult.

In coastal urban areas, sodium chloride (NaCl) from seasalt can react with HNO_3 to form sodium nitrate ($NaNO_3$) aerosol and hydrochloric acid (HCl) (R11). Ammonia can act to neutralize this acid as well, forming ammonium chloride (NH_4Cl) aerosol (R12).

$$NaCl_{(s)} + HNO_{3(g)} \leftrightarrow NaNO_{3(s)} + HCl_{(g)} \quad \text{R11}$$

$$NH_{3(g)} + HCl_{(g)} \leftrightarrow NH_4Cl_{(aq,s)} \quad \text{R12}$$

1.3 Inorganic PM in California

The state of California has both high human population and large agricultural production in close geographical contact and thus provides an ideal environment to study the formation of inorganic PM through the neutralization of atmospheric acids. Urban areas emit NH_3 and NO_x from mobile sources which mix with NH_3 from fertilizer and animal waste in agriculturally productive areas. Between mobile and agriculture sources, NH_3 emissions in California are some of highest in the country [*Goebes et al.*, 2003]. Sulfur dioxide (SO_2) is emitted from power generation in both areas. The topography of California, shown in Figure 1.2, plays an important role in controlling PM levels as the numerous valleys and mountain ranges allow for trapping and diversion of pollutants. Previous observational studies of PM formation in California have generally been concerned with two areas: the Los Angeles Basin and the Central Valley (comprised of the Sacramento Valley in the north and San Joaquin Valley in the south).

Figure 1.2: Topographic map of California with locations of valleys and major cities marked. [*Trump*, 2004]

Early studies of the Los Angeles (LA) Basin established the roles of emissions and meteorology in the formation of PM in this area. Observations made by *Russell and Cass* [1986] compare the urban core on the west side of the basin with sites downwind, to the east of agriculture operations, on a single day in August. Nitrogen dioxide (NO_2) and HNO_3 concentrations decrease from west to east, while NH_3 and aerosol nitrate (NO_3^-) levels increase. This supports the role of NH_3 emissions from agriculture in conversion of HNO_3 to NO_3^-. Diurnal trends at the most eastern site show peaks in NO_2, HNO_3 and NO_3^- during late morning and late afternoon, consistent with the timing of traffic. NH_3 shows a small peak during mid-morning with increasing concentrations after noon, which remain high for the rest of the day. This is likely from volatilization of NH_3 from manure during the afternoon due to higher temperatures. There is also evidence of aerosol transition back into the gas phase shortly after noon.

Chow et al. [1994] measured PM, gas precursors and meteorological parameters during the Southern California Air Quality Study (SCAQS), which took place in the same region in summer and fall of 1987. During the summer, HNO_3 is highest at the western sites and NH_3 and NO_3^- are highest at the eastern sites. This is consistent with *Russell and Cass* [1986]. SO_2 and SO_4^{2-} are relatively consistent throughout the region, but SO_4^{2-} does fall slightly in the east. Fall observations reveal a large increase in NO_3^- and decrease in HNO_3 throughout the region compared to summer, due to enhanced partitioning driven by colder ambient temperatures. Coarse PM ($PM_{10-2.5}$) makes up less than half of the total PM for most samples, and this portion decreased during the fall. Diurnally, PM mass concentrations peaked during the afternoon in the summer, but in fall the peak occurs in the morning. This indicates summer ventilation overnight and into the morning, which is absent during the fall due to the formation of temperature inversions near the surface.

NH_4^+, SO_4^{2-} and NO_3^- are more than 50 % of the fine PM ($PM_{2.5}$) mass in the summer in the LA Basin [*Chow et al.*, 1994], while average total $PM_{2.5}$ mass ranges from 25 μg m^{-3} near the coast to 64 μg m^{-3} downwind of agriculture NH_3 sources. In the fall, $PM_{2.5}$ mass increases, ranging from 73 μg m^{-3} near the coast to 86 μg m^{-3} to the east, with 90 μg m^{-3} observed in downtown LA. The percentage of this mass made up of NH_4^+, SO_4^{2-} and NO_3^- remains about the same. Chemical Speciation Network (CSN) measurements from 2005-2008 presented by *Hand et al.* [2012] show that NH_4NO_3 and $(NH_4)_2SO_4$ make up 60 % of $PM_{2.5}$ mass in LA in the summer, with total $PM_{2.5}$ mass of about 20 μg m^{-3}. These values drop slightly in the fall average, but November shows a peak of nearly 25 μg m^{-3} $PM_{2.5}$ in LA.

The formation of PM in the Central Valley is not as well studied, with most measurements focusing on the San Joaquin Valley (SJV). However, as both human population

and agriculture grow here at a rate higher than in the LA Basin, inorganic PM formation is becoming a larger concern [*Hall et al.*, 2008]. Generally, a similar mode of particle formation is found to occur here as in the LA Basin, only with a different mix of emissions and meteorological conditions. A wintertime fog water study by *Jacob et al.* [1986] showed that the acidity of the region is determined by local sources, with complete neutralization of acids closer to agricultural NH_3 emissions sources. Weather patterns play a large role in the overall aerosol concentration, as stagnation events during the winter trap air within the valley. Fog events during such times can contribute to new PM formation, but they also assist with removal by uptake of aerosol into the fog droplets which are deposited. NH_3 emissions are lowest during the winter, however, when such events occur.

Variations of precursor gases and resultant particles at 10 sites during the San Joaquin Valley Air Quality Study/Atmospheric Utility Signatures, Predictions, and Experiments (SJVAQS/AUSPEX) in summer 1990 are described by *Chow et al.* [1996] and *Chow et al.* [1998]. These measurements were made using filter-based methods. Throughout most of the study, NH_3, SO_2 and HNO_3 gas concentrations are equal to or larger than particle NH_4^+, SO_4^{2-} and NO_3^-. High HNO_3 levels are found at all sites, with highest NH_3 concentrations near agriculture operations. Maximum SO_2 is located at the southern end of the SJV near oil fields. SO_4^{2-} mass concentration dominates over that of NH_4^+ and NO_3^- at all sites. This is different from in the LA Basin where NO_3^- dominated. Higher NH_4^+ and NO_3^- concentrations do occur at sites closer to agricultural areas. Average total $PM_{2.5}$ mass ranges from 3 μg m^{-3} at the coast to 50 μg m^{-3} inland and south near high NH_3 and SO_2 sources and is made up largely by crustal species, with NH_4^+, SO_4^{2-} and NO_3^- making up 25 - 35 % of the mass. *Hand et al.* [2012] gives

summertime total $PM_{2.5}$ mass of 10 µg m^{-3} over the SJV and NH_4NO_3 and $(NH_4)_2SO_4$ as about 35 % of that mass.

All of these early studies conducted their observations using a network of ground stations on specific days, for relatively short periods of time. They used filter and denuder collection systems with time resolution between 1 and 6 hours, which were analyzed by techniques such as ion chromatography or automated colorimetry. These are time- and labor-intensive methods.

More recently, advancements have been made in measurement techniques, namely via the development on online techniques that increase the time resolution of sampling. *Neuman et al.* [2003] made high resolution (1 s) plane flight measurements over California using a Chemical Ionization Mass Spectrometer (CIMS) as part of the Intercontinental Transport and Chemical Transformation (ITCT) experiment in April and May 2002. This allows for analysis on a spatial resolution of 100 m at normal aircraft speeds and enhances the ability to study rapid chemical processes, such as NH_4NO_3 formation. One May flight during this campaign examined source regions and gas-to-particle conversion in the LA Basin. Results from this flight confirm and support previous results in this region. Under typical afternoon sea breeze conditions (clear, westerly winds), high HNO_3 and NO_x levels were measured directly downwind of the LA core. Further to the east, enhancements of NO_3^- and corresponding NH_4^+ concentrations are observed. SO_4^{2-} is always low in the region, less than NO_3^- and NH_4^+. The high resolution observations allow for the gas-to-particle conversion to be seen directly as the plane flies through a plume downwind of high agriculture NH_3 emissions. Farther yet to the east, over mountains which bound the LA basin, HNO_3 levels are reduced to near zero, showing nearly complete neutralization. NH_3 concentrations were not measured in this study, but calculations imply high

NH_3 levels over the expected emissions area. RH values during these conversion events are below the DRH and nearly all NO_3^- is in the particle phase.

High-temporal resolution HNO_3 and inorganic aerosol measurements were also made by Ellis et al. [in prep.] at an urban field site in Pasadena, CA, located at the northern end of the LA Basin, as part of the CalNex campaign (introduced below in Section 2.1). This site also included a new Quantum Cascade Tunable Infrared Laser Differential Absorption Spectrometer (QC-TILDAS) high resolution NH_3 instrument as well as HCl measurements due to the proximity to marine emissions. The observed diurnal trend of NH_3 corresponds with that of HNO_3, both of which peak in the afternoon, following daytime emission associated with traffic, warmer temperatures and transport from the Los Angeles city center. The NH_3 concentrations, however, do not correspond directly with other traffic pollutants such as carbon monoxide, as the NH_3 may have been lost to reaction or deposition during transport. NH_4^+ concentrations follow those of NO_3^- and SO_4^{2-}, which peak in the morning and afternoon, respectively. NH_3 concentrations are always high enough to neutralize SO_4^{2-} through NH_4^+ formation, but only certain meteorological conditions allow for NH_4NO_3 to form, particularly when temperature is lower. These results are largely consistent with similar situations on the western side of the LA Basin.

The study by *Neuman et al.* [2003] also discusses high resolution plane flight measurements over the SJV during the 2002 experiment. Gas-to-particle conversion is observed as the plane makes a descent from 4 km. Different regimes are observed above and within the boundary layer (below 2 km). At higher altitudes with colder temperatures, NH_4NO_3 particle is formed at the cost of NH_3 and HNO_3. Upon descent into warmer temperatures closer to the surface, this equilibrium shifts into the gas phase, reducing particle counts. As with in the LA Basin, RH values remain below DRH for NH_4NO_3. Level flights also compared concentrations

over the ocean, San Francisco and the SJV. Higher levels of NH_4^+, NO_3^- and $PM_{2.5}$ were found over SJV than over the ocean or San Francisco. HNO_3 concentrations were highest over San Francisco. SO_4^{2-} mass concentration is quite low and similar to that over LA. HNO_3, NO_3^- and $PM_{2.5}$ concentrations were about an order of magnitude lower over SJV than over the LA Basin, but the same gas-to-particle process was evident, especially when enhanced by agricultural NH_3 emissions.

Long term measurements have also been made at the Fresno Supersite, located in the SJV, in an effort to both test new instrumentation and understand trends in air quality in the region [*Watson et al.*, 2000]. In one study from this supersite, NO_3^- and SO_4^{2-} were measured by continuous and filter methods from 2000 - 2005 [*Chow et al.*, 2007]. Observed concentrations of NO_3^- were 6 - 9 μg m^{-3} higher in the winter (7 – 10 μg m^{-3}) than in summer (1 μg m^{-3}). In the winter, inversions kept NO_3^-, which formed overnight, aloft until mid-day. Summer NO_3^- levels peak in the morning before increasing temperatures force NH_4NO_3 back to the gas phase and allow for deeper mixing. No seasonal or long-term trends in SO_4^{2-} were evident in this study.

The ability to measure NH_3 concentrations from satellites is a new technique for studying areas where ground-based or plane flight observations may not always be present. For example, *Clarisse et al.* [2010] finds March - October average NH_3 concentrations ranging from 10 - 20 ppb in the SJV using the Infrared Atmospheric Sounding Interferometer (IASI). Limitations do currently exist regarding the accuracy of these retrievals, but improvements are expected in the future.

1.4 Modeling NH_x

Models can be used to interpret observations or as tools for policymakers to predict future trends. Validation of models with existing observations is important to improve the accuracy of these models. While a range of models, from thermodynamic partitioning to regional- and global-scale chemical transport, have been developed to represent the inorganic aerosol system and precursor gases, not many sets of robust ammonia observations have been used to validate them.

Many thermodynamic equilibrium models, such as ISORROPIA [*Nenes et al.*, 1998] and E-AIM [*Wexler and Clegg*, 2002], are used in order to predict the partitioning of inorganic gas and aerosol species. These models use ambient meteorology conditions, concentrations of specific species and known chemistry equilibrium parameters to solve the partitioning of the system. The specific species included, process complexity and calculation methods vary widely between models depending on their application. For example, a high level of accurate parameterization may be sacrificed for increased computational speed. The ISORROPIA II thermodynamic model [*Fountoukis and Nenes*, 2007] will be described in more detail in Sections 3.2 and 4.2.

Ellis et al. [in prep.] compares the CalNex surface observations in Pasadena, CA with ISORROPIA and E-AIM and shows two periods of model disagreement. During a nitrate-rich period, the models are biased low for NH_3 and HNO_3 gases under high RH conditions. In this case, the models move too much HNO_3 to the aerosol phase, decreasing the aerosol pH and causing NH_3 to move to aerosol to compensate. In a chloride-rich period, inclusion of chloride (Cl^-) in the model causes an increase in the already high model bias for NH_3. However, model agreement with HNO_3 observations is simultaneously improved. This indicates that perhaps

additional species such as organic acids may be reacting with NH_3. Inclusion of Cl^- also increases the model pH, partitioning more NH_3 to the gas phase. Gas-particle partitioning is very sensitive to aerosol pH, and inclusion of cations such as sodium (Na^+) in these models have been implemented to improve calculated aerosol pH. Inclusion of organic acids could further improve this aerosol pH.

Observations, ranging from 1 - 24 hr resolution, from the California Regional $PM_{10}/PM_{2.5}$ Air Quality Study (CRPAQS) in 2000 are compared with the CMAQ-MADRID 1 model, which links an aerosol model with a chemical transport model, by *Zhang, et al.* [2010b]. Gas phase measurements included in this study are hourly SO_2, 3 - 8 h average HNO_3 and NH_3 and 24 h average NH_3. During this wintertime study of the SJV, the model over-predicts NO_3^- by about 40 % and NH_4^+ by 20 %. SO_2 is over-predicted and NO_y and NH_3 are under-predicted by the model. Despite the measurements, they cannot attribute the problem to any one source, but state it may be due to underestimates in gas precursor emissions, problems with gas-particle partitioning or errors in the meteorological variables.

2. Research Objectives

In this study, we aim to use the GEOS-Chem model (described below in Section 3.2) to examine inorganic PM formation and ammonia in California after validation and modification using high-resolution aircraft measurements made during the CalNex campaign.

Research Objectives:

1. Compare and contrast the formation of PM through the reaction of acids with ammonia in two California regions: urban (the LA basin) and agricultural (Central Valley).
2. Address significance of excess agriculture ammonia, through quantification of export to systems downstream.
3. Identify weaknesses in the model's ability to represent this system and quantify sensitivities to key processes.

3. Tools

3.1 CalNex Airborne Observations

The CalNex field study took place during May and June 2010 in California and the nearby Pacific coastal waters. The purpose of CalNex was to examine issues at the "nexus" of climate change and air quality, where decision-makers may be faced with coupled relationships between both issues. Among the science questions to be addressed were improving emissions inventories, identifying source contributions to chemical species, investigating chemical reaction processes, and understanding transport processes along the coast, in cities and throughout agricultural valleys. This campaign was funded by the National Oceanic and Atmospheric Administration (NOAA), the California Air Resources Board (CARB) and the California Energy Commission (CEC) (www.esrl.noaa.gov/csd/projects/calnex/).

CalNex included an assortment of deployment methods and instruments. Measurement platforms included the NOAA WP-3D and Twin Otter Remote Sensing aircraft, the *R/V Atlantis* mobile platform, ground-level supersites in Bakersfield and Pasadena and an ozonesonde network. The majority of analysis for this work consists of in-situ observations from 18 NOAA WP-3D aircraft flights which took place throughout California. These flights collected approximately 7000 minutes worth of data, and Figure 3.1 shows their track locations. The altitude of the plane during these flights varied from surface-level up to about 6 km, with much of the flight time dedicated to the lower troposphere (below 3 km). Limited flight time precluded a good characterization of the diurnal variation in concentrations throughout the regions with only about 20 % of flight time at night.

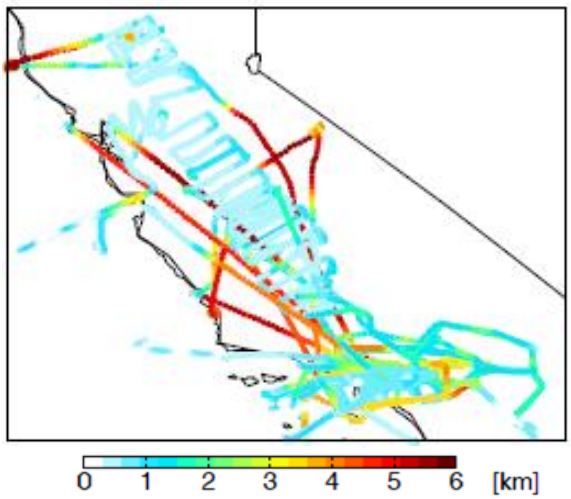

Figure 3.1: Location of 18 NOAA WP-3D flights during CalNex, colored by altitude, used in this analysis.

The instruments aboard the NOAA WP-3D were coordinated by the NOAA Earth System Research Laboratory (ESRL) Chemical Science Division and measured a variety of meteorological parameters, gaseous chemical species mixing ratios and aerosol species mass concentrations. Primary interest for this analysis of the inorganic gas-particle system concerns gaseous NH_3, SO_2, and HNO_3 and particle ions NH_4^+, SO_4^{2-}, and NO_3^-. NH_3 was measured by chemical ion mass spectrometry (CI-MS) [*Nowak et al.*, 2007] with an average uncertainty of ±(30 % + 0.2 ppb) (calibration uncertainty + measurement imprecision). SO_2 was measured by pulsed UV fluorescence [*Ryerson et al.*, 1998] with an uncertainty of ±(15 % + 0.5 ppb). HNO_3 was measured by CI-MS [*Neuman et al.*, 2002] with an uncertainty of ±(15 % + 0.052 ppb). Since gas concentrations are calculated by differencing the measured signal from an interpolated background concentration, negative values may be returned. The sub-micron particle ions were measured by aerosol mass spectrometry (AMS) [*Jayne et al.*, 2000; *Jimenez et al.*, 2003; *Bahreini et al.*, 2003] with an average uncertainty of ±30 %. The aerosol concentrations are reported in µg sm^{-3}, where standard conditions are set to 1013.25 hPa and 0 °C. Additional measurements discussed here include particle chloride Cl^-, measured by AMS. The gas species

and meteorology parameters were reported at 1 s resolution and the particle ions at 10 s resolution. All observations are averaged to 1 min prior to analysis as described below.

These observations during CalNex, particularly for NH_3, are also described and used in analysis of the inorganic aerosol system in the LA Basin by *Nowak et al.* [2012]. Similar high-resolution measurements were also made by a WP-3D instrument deployment over Houston during the 2006 Texas Air Quality Study [*Nowak et al.*, 2010].

3.2 GEOS-Chem Model Simulation

The GEOS-Chem chemical transport model (www.geos-chem.org) is used to interpret the CalNex plane flight observations and investigate the role of NH_3 in the formation of PM in California and export of excess NH_3. GEOS-Chem is driven by assimilated meteorology from the NASA Global Modeling and Assimilation Office (GMAO). The model uses emission inventories for both organic and inorganic species and contains parameterizations for chemical reactions, the partitioning of aerosols, transport, and deposition.

For this analysis, a global simulation of GEOS-Chem v9-01-01 is run for 2010 at 2° x 2.5° horizontal resolution with 47 vertical layers. This global simulation has the capability to output boundary conditions for a nested sub-region of the globe at higher resolution [*Wang et al.*, 2004; *Chen et al.*, 2009]. Such a nested simulation is run over North America for 2010 at 0.5° x 0.667°. Figure 3.2 shows the comparison of horizontal grid resolutions mentioned above and the location of the North America sub-region. The ability to assign a nested region at higher resolution allows for analysis of smaller horizontal-scale features without dramatically increasing computational runtime.

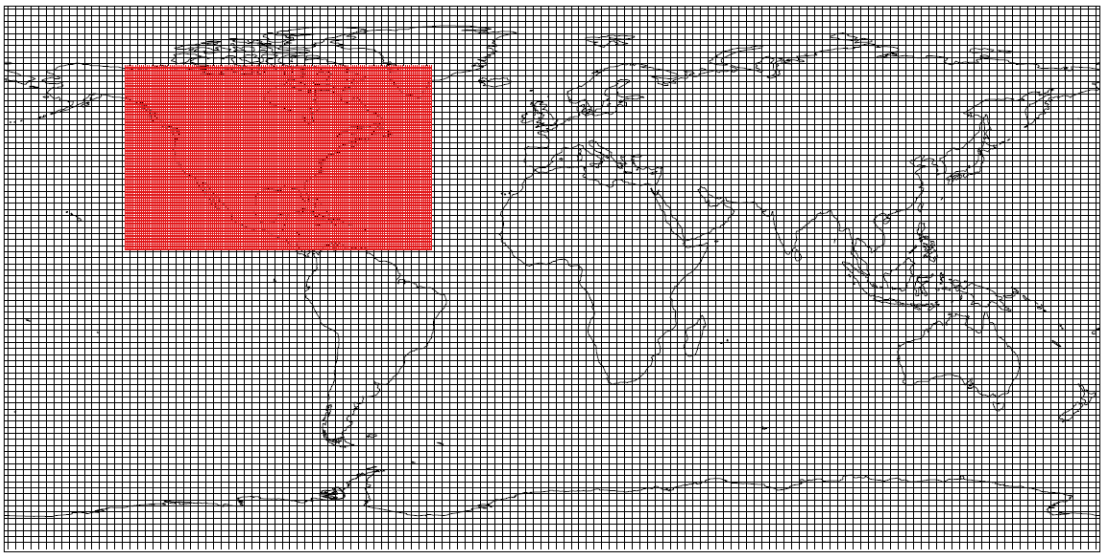

Figure 3.2: GEOS-Chem 2° x 2.5° resolution gridboxes (black) overlaid by nested North America sub-region at 0.5° x 0.667° resolution (red).

The sulfate-nitrate-ammonium (SNA) aerosol system was introduced into GEOS-Chem and coupled to gas-phase chemistry by *Park et al.* [2004]. Gas-aerosol phase partitioning of these species is handled by the thermodynamic equilibrium model ISOROPPIA II, developed by *Fountoukis and Nenes* [2007] and added to GEOS-Chem by *Pye et al.* [2009]. ISOROPPIA II uses ambient temperature and RH as input along with the concentrations of gases (NH_3, SO_2 and HNO_3) and aerosols (NH_4^+, SO_4^{2-}, NO_3^- and Na^+ and Cl^- from accumulation mode sea salt) to establish thermodynamic equilibrium between gas and aerosol phases. The implementation of ISOROPPIA II into GEOS-Chem assumes that the species exist on the upper, metastable branch of the hygroscopic hysteresis curve, meaning the transition from aqueous to solid equilibrium occurs at the ERH, rather than the DRH. This assumption only presents an issue at upper altitudes, where RH does not regularly reach high values [*Pye et al.*, 2009]. Wet and dry deposition processes are also parameterized and included in GEOS-Chem. These removal methods will be discussed in greater detail in Section 4.3.

Over the United States, anthropogenic emissions in GEOS-Chem follow the Environmental Protection Agency's National Emissions Inventory for 2005 (EPA NEI-2005, ftp://aftp.fsl.noaa.gov/divisions/taq/emissions_data_2005). The NEI-2005 used in GEOS-Chem is a compilation of NEI-2005 on-road and non-road mobile sources, NEI-2002 area sources and August 2006 continuous emissions monitoring system (CEMS) point sources with NEI-2002 point sources at non-CEMS locations. Emissions rates in NEI-2005 are reported for an August weekday, and these rates are scaled in GEOS-Chem as required by variability in an individual species. For SO_x (SO_2 + SO_4^{2-}) and NO_x (NO + NO_2), an annual scale factor based on emissions trends and monthly and weekday/weekend scaling based on NEI-1999 is applied. Only monthly scaling is applied to NH_3. Figure 3.3 shows the NEI-2005 anthropogenic emissions of NH_3, SO_x and NO_x anthropogenic emissions for May 2010 over both the continental U.S. and zoomed in to California. Anthropogenic NH_3 emissions are dominated by agricultural areas, such as the Midwest, Great Plains and the Central Valley of California. Secondary NH_3 emission hotspots

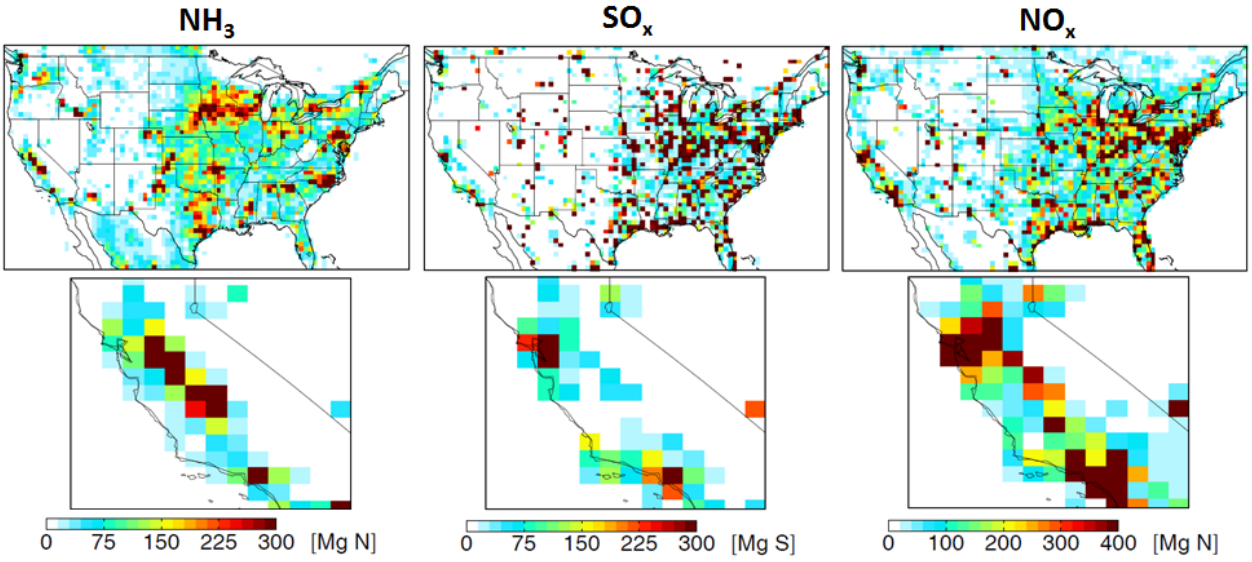

Figure 3.3: Total May 2010 anthropogenic emissions rate for NH_3, SO_x and NO_x in the United States (above) and California (below).

occur over cities with high automobile usage, such as Los Angeles. Anthropogenic SO_x emissions are a sign of electricity production and industrial processes, and high SO_x emissions values are seen from population centers and isolated power plants. Near the coast, SO_x can also be significantly emitted by shipping activities. For example, shipping activities account for about 46 % of SO_2 emissions in the area around LA according to NEI-2005. Anthropogenic NO_x emissions are largely from mobile sources in urban areas and are particularly dominant in California.

Biofuel emissions over the United States generally follow the NEI-1999 inventory, which provides both weekday and weekend emissions values. This is true for both SO_x and NO_x. NH_3 biofuel emissions, however, are from the 1990 Global Emissions Inventory Activity (GEIA) as described by *Bouwman et al.* [1997]. Biofuel refers to burning of fuel for domestic use, such as heating and cooking by wood or coal.

In the standard GEOS-Chem v9-01-01, biomass burning emissions follow the Global Fire Emissions Database (GFED2) [*van der Werf et al.*, 2009], which gives monthly global emissions values, but is not available beyond 2008. As we are interested in 2010, we implement the Fire INventory from NCAR (FINN) [*Wiedinmyer et al.*, 2011] in GEOS-Chem, which provides daily global coverage of biomass burning emissions. The assumed point FINN emissions are gridded to both resolutions mentioned above for all available species, including NH_3, SO_2 and NO_x.

Lightning NO_x has been updated in GEOS-Chem v9-01-01 by *Murray et al*. [submitted] to provide more appropriate scaling. All other relevant emissions, such as soil NO_x, follow as described by *Pye et al.* [2009]. In this study, particular attention is given to the emission inventories for NH_3. There are four NH_3 emissions categories in GEOS-Chem: anthropogenic, biofuel and biomass burning (introduced above), as well as natural. Natural NH_3 emissions, like

biofuel, are from the 1990 Global Emissions Inventory Activity (GEIA) as described by *Bouwman et al.* [1997]. Biomass burning is the only NH_3 emission category that varies daily. Other source categories vary monthly, and in the case of anthropogenic NH_3 emissions, a monthly scale factor is applied to all areas and sectors equally. Figure 3.4 compares the magnitudes and trends of the four NH_3 emissions categories in both the United States (US) and California. Anthropogenic sources provide the largest portion and largest annual variability of NH_3 emission in the both regions. A summer peak is observed, largely due to increased farm application activity and higher volatility corresponding with higher temperatures. The trend in both regions is identical, as the same anthropogenic scaling factor is applied everywhere. Natural sources have moderate variability and are the second largest category after anthropogenic sources. They make up a larger portion of NH_3 emission over the entire US than in California alone. Biofuel has small variability, but does show a peak in the winter due to increased heating needs. This is similar in both regions. The magnitude of the total US biofuel NH_3 emissions is larger than total US biomass burning NH_3 emissions, although the highly variable biomass

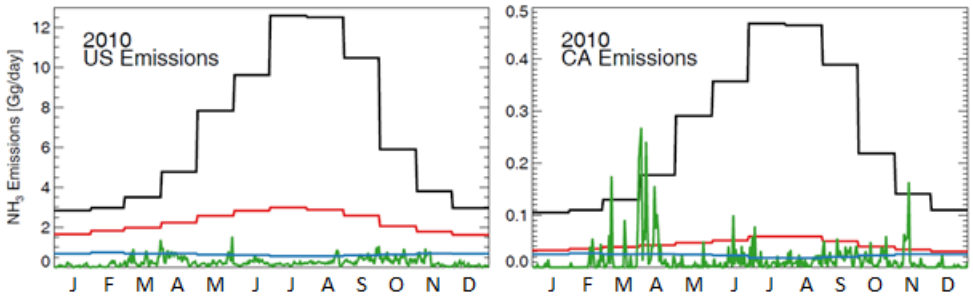

	US	CA	
Anthropogenic	2.4	.091	Tg yr^{-1}
Natural	.85	.016	Tg yr^{-1}
Biofuel	.23	.006	Tg yr^{-1}
Biomass Burning	.09	.008	Tg yr^{-1}

Figure 3.4: Annual trends of NH_3 emissions categories in GEOS-Chem for the United States (top left) and California (CA) (top right) for 2010: anthropogenic (black), natural (red), biofuel (blue), biomass burning (green) and annual total NH_3 emissions for each region and category (bottom).

burning source does eclipse biofuel emission in a few cases. There is a general increase in biomass burning activity in the spring and fall. This increase is much more pronounced in California, a chief area of wildfire activity in the US. At times the biomass burning source is even larger than the anthropogenic source for that day, but this seldom occurs, such that biomass burning is the second smallest source category in California.

Several previous studies have used GEOS-Chem to examine formation and impacts of inorganic aerosol. *Park et al.* [2004] compared an earlier version of GEOS-Chem with SNA aerosol concentration and deposition observations from the IMPROVE, CASTNET and NADP ground networks in the United States. They find that SO_4^{2-} is well represented both spatially and temporally, while NO_3^- and NH_4^+ are too high in the model during summer and fall. A lack of NH_3 prohibits complete neutralization of HNO_3 in most areas. The model was then used to assess the effects of transboundary pollution on visibility in the US, concluding that complete elimination of domestic sources will not reduce SNA concentrations to background levels. *Pye et al.* [2009] use GEOS-Chem coupled to the GISS climate model to examine changes in SNA aerosol due to climate and emission changes. They find that concentrations of inorganic aerosol at IMPROVE and CASTNET sites are widely under-predicted over the entire United States. Season-averaged normalized mean bias ranges up to -50 % for SO_4^{2-}, -41 % for NO_3^- and -32 % for NH_4^+. In particular, the authors speculate that underestimated NH_3 emissions can account for the low bias in simulated NO_3^- at sites in southern California. However, sensitivity analyses indicate that total ammonia and total nitrate emissions would need to be increased by unrealistically high levels (5 - 10 times current emissions inventories), to reproduce the observed nitrate concentrations. They conclude that NH_3 inventory errors are not the primary reason for this discrepancy and instead point to missing processes and low resolution (horizontally 4° x 5°).

Recently, *Zhang et al.* [2012] investigated nitrogen deposition over the United States using the high-resolution nested version of GEOS-Chem. Comparison of model output with a suite of ground-based observations shows little bias in NH_x (NH_3 + NH_4^+) and SO_4^{2-} concentrations. Positive bias exists for HNO_3, NH_4^+ and NO_3^- which they suggest may be associated with excess production of HNO_3 from N_2O_5 hydrolysis. Model results indicate that about twice as much nitrogen deposited in the United States is from oxidized forms (NO_y) than from reduced forms (NH_x). Domestic anthropogenic emissions contribute to a large portion of this NO_y and NH_x deposition in the United States.

Given limitations of previous studies, which focus largely on global or national scale issues using a low resolution simulation, with limited evaluation of gas-phase species, the airborne observations made during CalNex provide a unique application of GOES-Chem in order to analyze the SNA system and PM formation over a specific, high emission area, California. In our study, high spatial and temporal resolution inorganic gas and aerosol observations at various altitudes are used to evaluate and investigate the nested high-resolution GEOS-Chem simulation. This is especially important for the case of gaseous ammonia, which has a very limited reliable observational record in such context. Optimization of the fine-scale model will allow for better assessment of PM levels and effects of excess NH_3 across the region.

4. Model Evaluation

4.1 Initial Comparison to Observations

The concentrations of species simulated with GEOS-Chem are output along the 3-dimensional path of the 1 min averaged CalNex plane flight observations. Both the model and observed concentrations are then averaged over the coarser of this 1 min timestep or the resolution of the model grid. This averaging provides a more accurate comparison by averaging samples located within the same model timestep and spatial gridbox. Figure 4.1 shows the average surface NH_3 concentration for May 2010 over California for both the coarse 2° x 2.5° standard resolution and the North America nested 0.5° x 0.667° resolution. The nested grid is able to resolve more of the smaller-scale spatial features, which is especially important given the topography of California. Specifically, the nested resolution in Figure 4.1 better resolves the Central Valley of California and the LA basin region. Figure 4.2 compares vertical profiles of the grid-averaged model output with the CalNex observations of SO_2 concentration for both resolutions during the entire study period. Without going into too much detail concerning the discrepancies between the model and observations, it is clear that the nested model resolution provides a better comparison to the observations. The more highly resolved spatial features in the

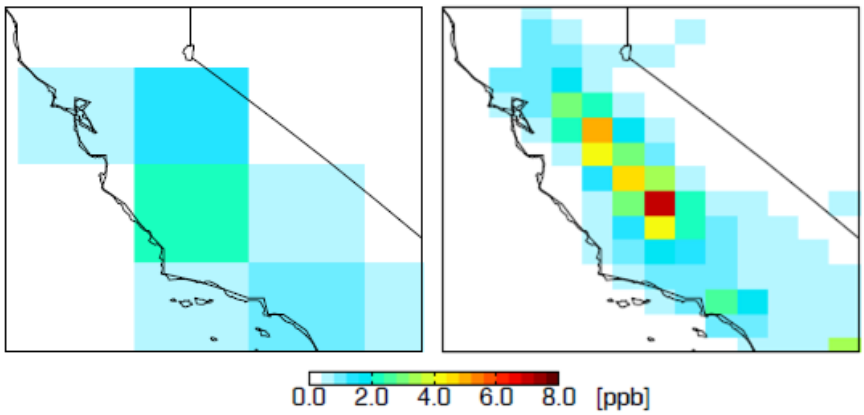

Figure 4.1: Monthly mean standard GEOS-Chem NH_3 surface concentrations for California during May 2010. 2° x 2.5° resolution (left). 0.5° x 0.667° resolution (right).

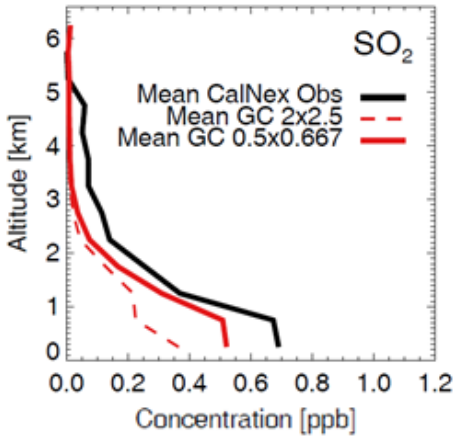

Figure 4.2: Vertical profiles of SO_2 during CalNex. Comparison of mean observations and model output using 2° x 2.5° and 0.5° x 0.667° resolution.

nested resolution lead to improved point concentration quantification. From this point forward, all analysis will be done using the nested resolution model output.

Point-by-point examination of the CalNex observations shows that many isolated plumes of high species concentration are present throughout the study. It is not possible for a coarse Eulerian model, such as GEOS-Chem, to reproduce these plumes, as concentrations diffuse through a grid box [*Rastigejev et al.*, 2010]. Given that the aircraft does not uniformly sample a grid box, any such plume can bias the comparison with model concentrations. The skewed nature of the NH_3 observations compared to the model output is shown in the histogram of concentration frequency in Figure 4.3. Thus, all averaging done in these comparisons will use median, rather than mean, as a test of model performance. Once applied, Figure 4.3 compares the mean and median vertical profiles of the observed and simulated NH_3 concentrations. We see here that the model median and mean are in close agreement, while the skewness of the observed concentrations leads to a large difference in these quantities. The median removes the bias created by these high concentration plumes, often bringing the comparisons closer into

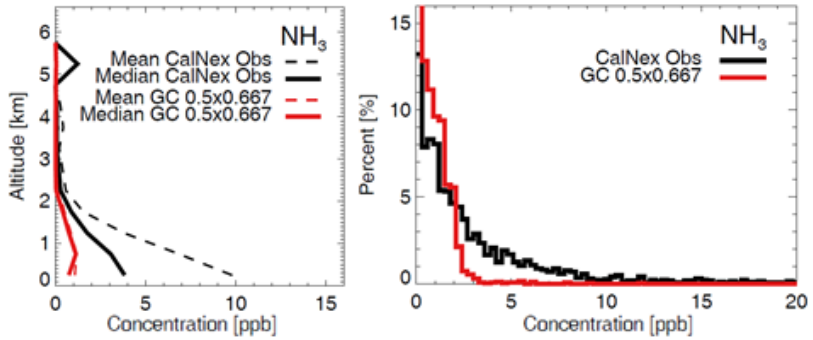

Figure 4.3: Vertical profile comparison of mean and median NH_3 CalNex observations and GEOS-Chem model output using 0.5° x 0.667° resolution (left). Histogram comparison of NH_3 concentration frequency for CalNex observations and GEOS-Chem model output using 0.5° x 0.667° resolution (right).

agreement. These characterizations regarding resolution and averaging are consistent across and applied to all species examined in this study.

Rather than consider the entire CalNex campaign area as a whole, we divide the analysis into the two regions mentioned and examined by previous studies: the LA Basin and surrounding area, referred to here as the "City" region, and the Central Valley, referred to here as the "Valley" region. Splitting the data into two large regions retains the significance achieved through analysis of many data points, while allowing for examination of the inorganic aerosol system under very different circumstances. The City region is dominated by NO_x and NH_3 emissions from vehicles and industrial SO_x, especially within the Los Angeles core area. Lower levels of agricultural NH_3 emission are found outside this core area. NH_3 emissions from agriculture dominate the Valley region. High NO_x emissions are seen over urban areas in the Valley, and SO_x emissions are quite low here compared to the City. Figure 4.4 shows the location of the points in these regions relative to the whole campaign. There are about twice as many points in the City region as in the Valley. Measurements taken outside of these two primary regions (in grey in Figure 4.4) are not included in our analysis.

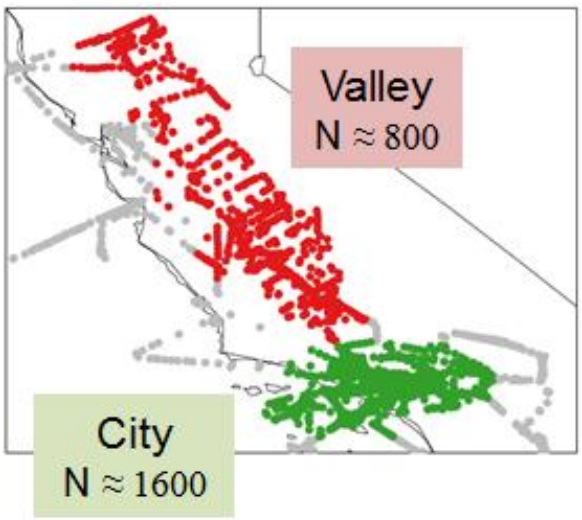

Figure 4.4: CalNex points associated with City region (green) and Valley region (red).

Point-by-point comparisons of the observations and model for the six main species of interest (gases: NH_3, SO_2, HNO_3 and particle ions: NH_4^+, SO_4^{2-}, NO_3^-) are shown in Figure 4.5. These have been split into the two regions mentioned above. The model reproduces only a modest fraction of the observed variability for many species (low linear regression coefficients (R) are generally present through all species in both regions). More scatter is seen over the same concentration range in the City than in the Valley, with the only R value over 0.5 for HNO_3 in the Valley. These figures also illustrate the wide range of conditions sampled across California, with observed concentrations ranging 1 to 2 orders of magnitude. Comparison of the regression line slope with the 1:1 line allows us to make general statements regarding the model bias.

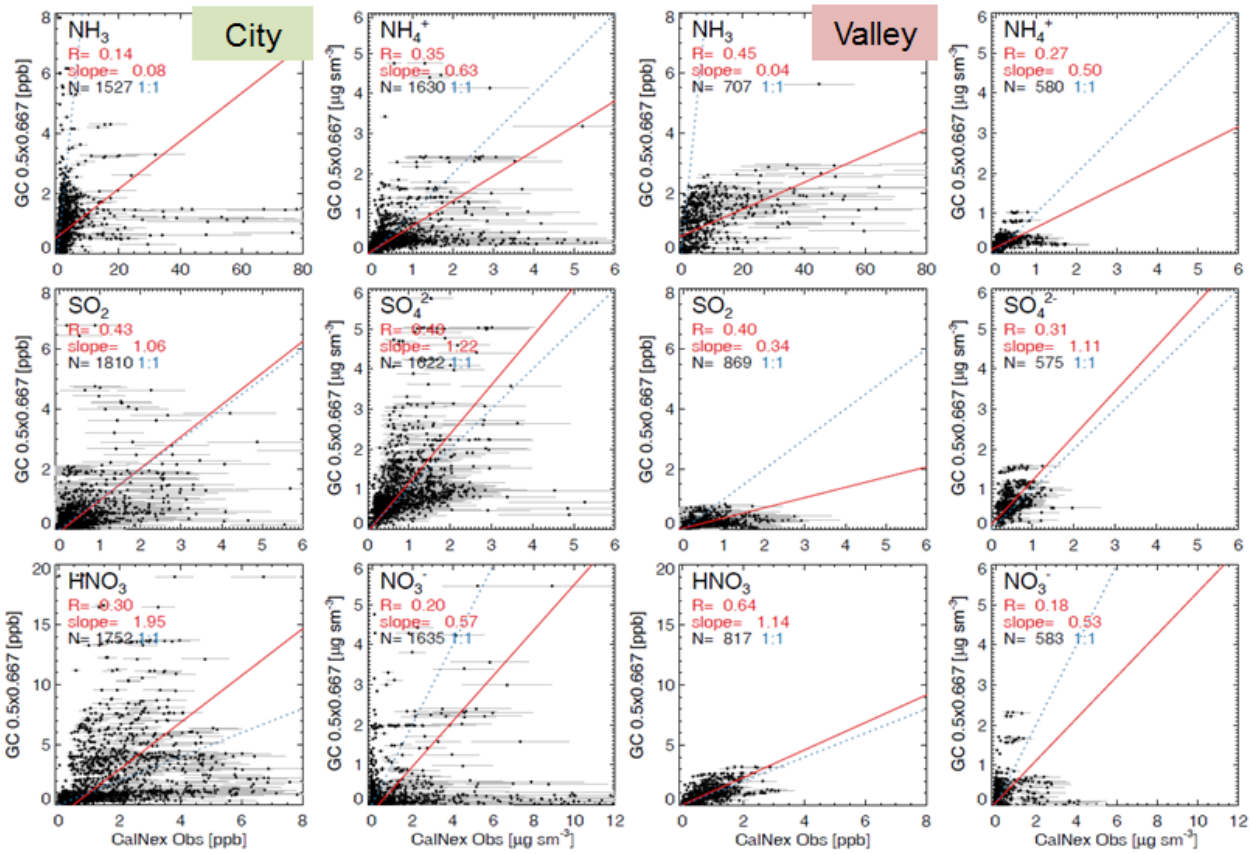

Figure 4.5: Scatterplots comparing CalNex plane flight observations and GEOS-Chem model output along those flight paths. Points have been split into City region (left) and Valley region (right). Reduced major axis regression line shown in red and slope = 1 line in blue (dashed). Observational uncertainty for each point shown in grey.

Regression slopes under (over) 1 indicate low (high) bias in the model compared to the CalNex observations. In both the City and the Valley, NH_3 is greatly under-predicted, and NH_4^+ and NO_3^- are moderately under predicted. SO_x levels are generally reproduced in the City, while SO_2 is under-predicted in the Valley. HNO_3 in the City is the only example of significant over prediction. The measurement uncertainties of the observations are also plotted for each point in Figure 4.5. Uncertainties on individual measurements are large. Where ambient concentrations were low, some point observations, especially in NH_3, SO_2 and NO_3^-, have values below zero. However, positive concentrations fall within the uncertainties of these points.

Figure 4.6 shows a further detailed comparison of the spatial gradients across the region by plotting the median concentrations at all altitudes of both observations and the model. Model concentrations of NH_3 are biased quite low over the Valley, up to 20 ppb in some areas, while the NH_3 under-prediction in the City is not nearly as large. SO_2 in the model is noticeably low in the Valley as well, especially in the southern Valley. Model output for HNO_3 and all three aerosol species is slightly low in the southern Valley, but a bit high on the northern end. HNO_3, NH_4^+ and NO_3^- are slightly low in the City. Outside of NH_3, the model biases are all less than 4 ppb (for the gas-phase species) or 4 µg sm^{-3} (for the particle-phase species).

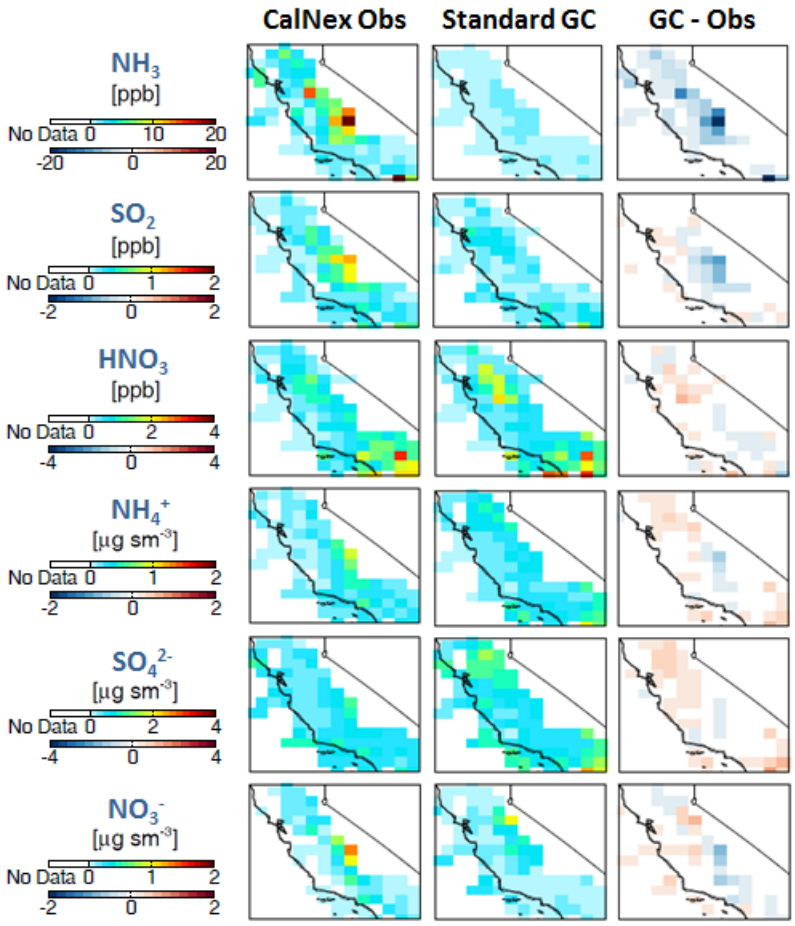

Figure 4.6: Median CalNex plane flight observations (left column) and median GEOS-Chem model output along those flight paths (center column) averaged vertically over each grid box, corresponding to the model nested resolution grid boxes, for gas and aerosol species. Difference between observations and model is in the right column.

Comparisons of the vertical profile are made by binning the observation and model points by altitude every 500 m from the surface up to 6.5 km and calculating the median. As above, these vertical profiles in Figure 4.7 are split by region. The number of points in each bin varies from the 100s near the surface to less than 10 at 6 km. Bins with fewer than two observations are not plotted. The standard deviation of the observations in each bin is also shown as a bar to denote the high degree of observed variability. In general, both the observations and the simulation agree that species concentrations decrease with increasing altitude due to surface sources and the short lifetimes of these species. Exception to this occurs in the near-surface

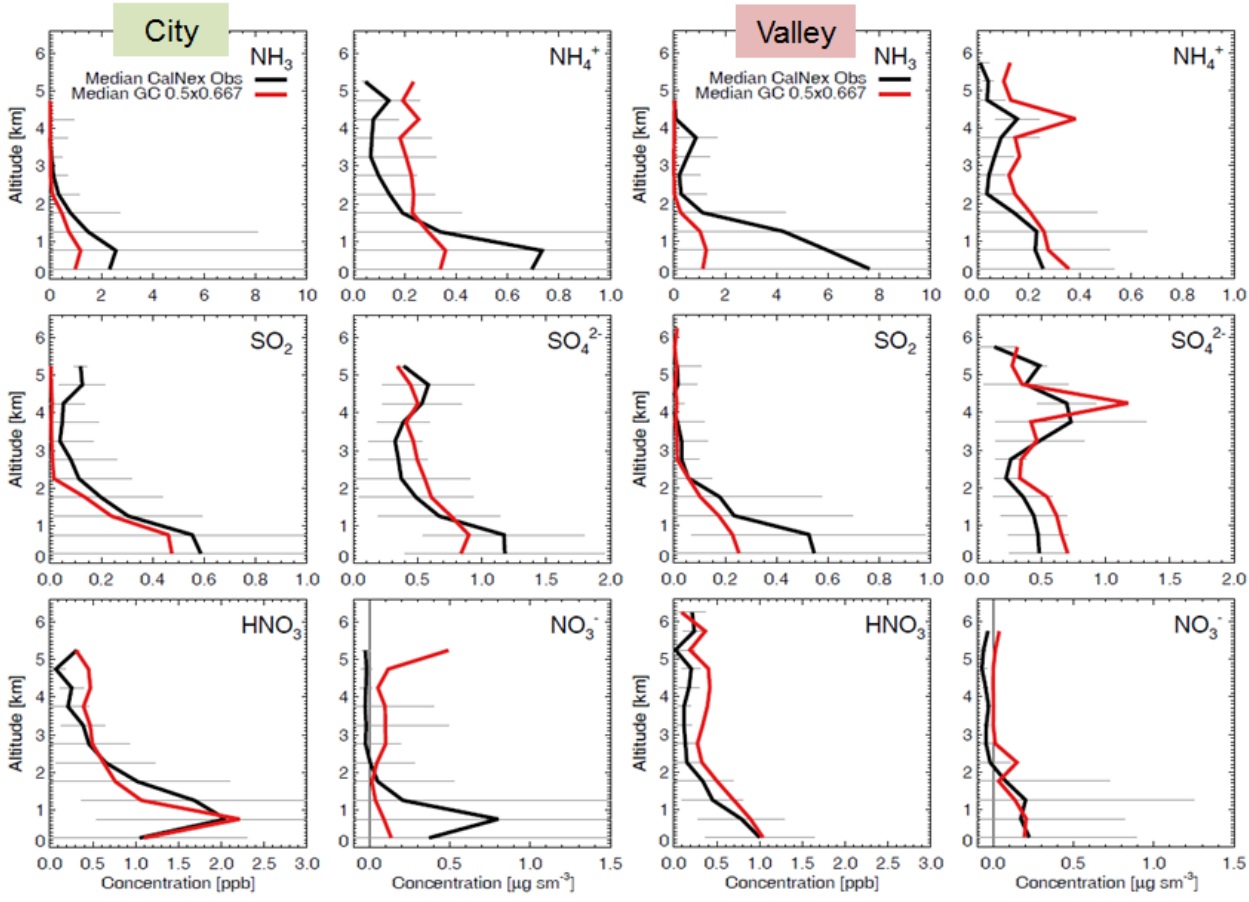

Figure 4.7: Vertical profiles of median CalNex plane flight observations (black) and median GEOS-Chem model output along those flight paths (red) averaged in 500 m altitude bins. Split into City region (left) and Valley region (right). The standard deviation from the mean and applied to the median is shown in grey.

layer, where deposition can play a role in the concentration (see Section 4.3). Standard deviation is high near the surface when the observed concentrations have a large spread due to the variation of sample locations (NH_3 in both regions). Many samples of consistent observed concentration lower this standard deviation (HNO_3 and SO_4^{2-} in the Valley). Model bias in the concentration for individual species mirrors the discussion of the scatterplots and gridded fields discussed above, especially in the lowest 2 km. Model NH_3 is quite low compared to observations in the Valley region, with a bias of about 6 ppb at the surface. This low bias in NH_3 is only 1 ppb in the City. Model SO_2 is biased low by about 0.25 ppb in the Valley, while the comparison is good in the City. HNO_3 compares well in both regions, suggesting that the scatterplots of the City concentrations in Figure 4.5 may be skewed by the outliers. Modeled aerosols at the surface are all low in the City region, while NH_4^+ and SO_4^{2-} are slightly high in the Valley. This is different from Valley aerosol scatterplots in Figure 4.5 which show a low model bias, again likely due to skewed outliers.

The meteorological parameters temperature and relative humidity (RH) are also relevant to the analysis of this system, given that they affect phase partitioning of ammonium nitrate. CalNex observations and simulated concentrations are compared through the same averaging method as the previously mentioned species. Recall that the meteorological values used in the model are prescribed from GEOS-5 assimilated meteorology and are not calculated within the GEOS-Chem model itself. Figure 4.8 shows scatterplot, vertical profile and histogram comparisons of temperature and RH split into the City and Valley regions. The median model temperature profile is biased low by about 1 °C in both regions. However the model and observations are highly correlated, with linear regression slopes close to 1. The frequency histograms support this shift of about 1 °C in the City, but also show that differences of up to 5

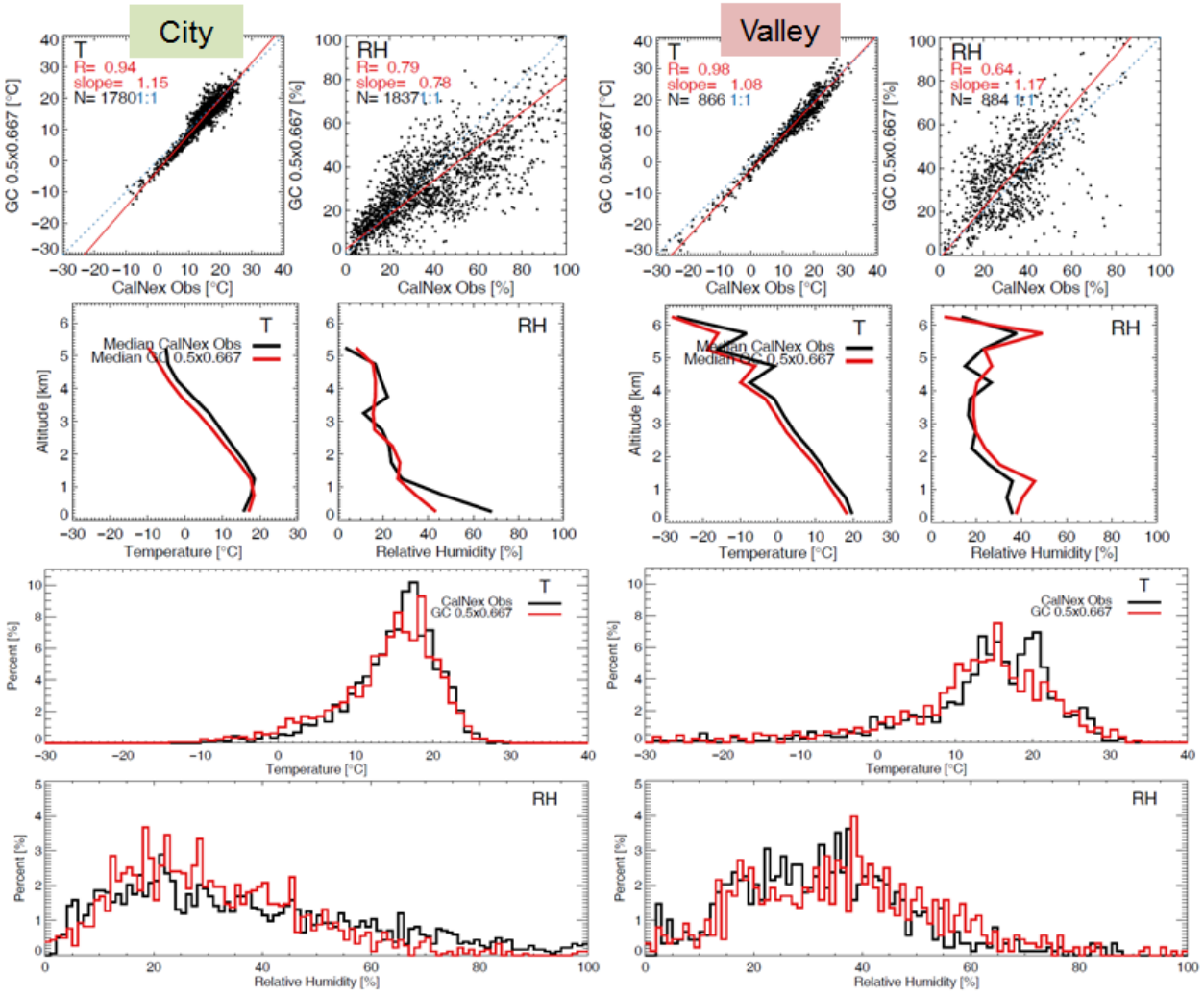

Figure 4.8: Comparison of CalNex plane flight observations and GEOS-Chem model output along those flight paths for temperature (T) and relative humidity (RH). Split into City region (left) and Valley region (right). Top: Scatterplots. Middle: Vertical profiles. Bottom: Histograms.

°C can occur in the Valley. More frequent extreme temperatures are found in the Valley than in the City. The RH comparison is slightly more scattered, but still quite good. The median model bias in RH for individual observations ranges from about 5 - 10 %, in both directions, but no mean bias is evident. The distribution of model RH seems to be shifted slightly lower in the City and higher in the Valley.

Other chemical species relevant to this system include Na^+ and Cl^-. Largely present near seawater as a portion of seasalt, they can react with HNO_3 (H_2SO_4) to form $NaNO_3$ (Na_2SO_4)

aerosol and HCl. This reaction both reduces the concentration of HNO_3 (H_2SO_4) and creates additional acid which can be neutralized by NH_3. The net effect on aerosol concentration depends on the extent of this displacement and the equilibrium conditions of the reactions. Figure 4.9 shows median vertical profile comparison of observations and model for Cl^-. Na^+ was not measured during CalNex and is part of the same seasalt species in GEOS-Chem as Cl^-. The model over predicts Cl^- at the surface in both the City and Valley, however these concentrations are quite small. Almost no Cl^- is observed in the Valley, which is far from marine sources.

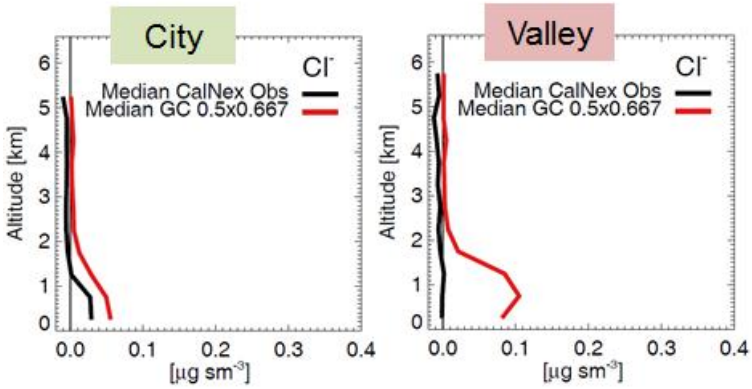

Figure 4.9: Vertical profile comparison of CalNex plane flight observations and GEOS-Chem model output along those flight paths for Cl^-. Split into City region (left) and Valley region (right).

The discrepancies between the CalNex observations and GEOS-Chem model output identified above could be due to several factors within the model. In the following sections, we discuss these model elements, diagnose concentration sensitivities due to model uncertainties and propose solutions to reconcile the differences.

4.2 Gas-to-Particle Partitioning

The ISORROPIA II thermodynamic equilibrium model in GEOS-Chem determines both the partitioning of NH_3 into NH_4^+ in order to neutralize SO_4^{2-} and the partitioning of NH_4NO_3

between the aerosol and gas phases. This is based on the ambient temperature and RH and model concentrations of NH_x, SO_4^{2-}, total nitrate (TNO_3), Na^+ and Cl^-. (Potassium (K^+), calcium (Ca^{2+}) and magnesium (Mg^{2+}) ions are not present in GEOS-Chem, and their concentrations are set to be zero in ISORROPIA II.) Given the assumption of metastable equilibrium used in the model, NH_4NO_3 particles remain deliquesced through the lowest ambient RH levels. For example, assuming an NH_4NO_3 ERH of 15%, which decreases further when a particle is more acidic or the NH_4NO_3:$(NH_4)_2SO_4$ ratio increases, 84% of CalNex observation points in the City and Valley remain deliquesced. Thus, both temperature and RH play a role in the formation of NH_4NO_3 throughout a large portion of the region.

Comparisons to observed meteorology above showed a consistent model bias of about 1 °C for temperature and an error on individual points of 5 - 10 % for RH. In order to determine the effects that these errors could have on model concentrations of our species of interest, we perform a series of sensitivity simulations where the meteorological inputs into ISORROPIA II are varied. These simulations were run for +/- 1 °C and +/- 10 % RH. Figures 4.10 and 4.11 show vertical profiles of the six main species as in Figure 4.7, but shaded areas have been added to show the variation in model output with this varied input into ISORROPIA II. Figure 4.10 shows sensitivity to temperature and Figure 4.11 shows sensitivity to RH. As expected, only changes to the partitioning of NH_4NO_3 in the model are evident. Examination in molar units confirms that species are being directly moved between gas and aerosol ($NH_3 \leftrightarrow NH_4^+$ and $HNO_3 \leftrightarrow NO_3^-$). The sensitivity to changes in 10 % RH is greater than those to 1 °C, but these changes are still quite small compared to species which display large model bias. Based on these vertical profiles, we can say that model bias in temperature and RH during CalNex does not

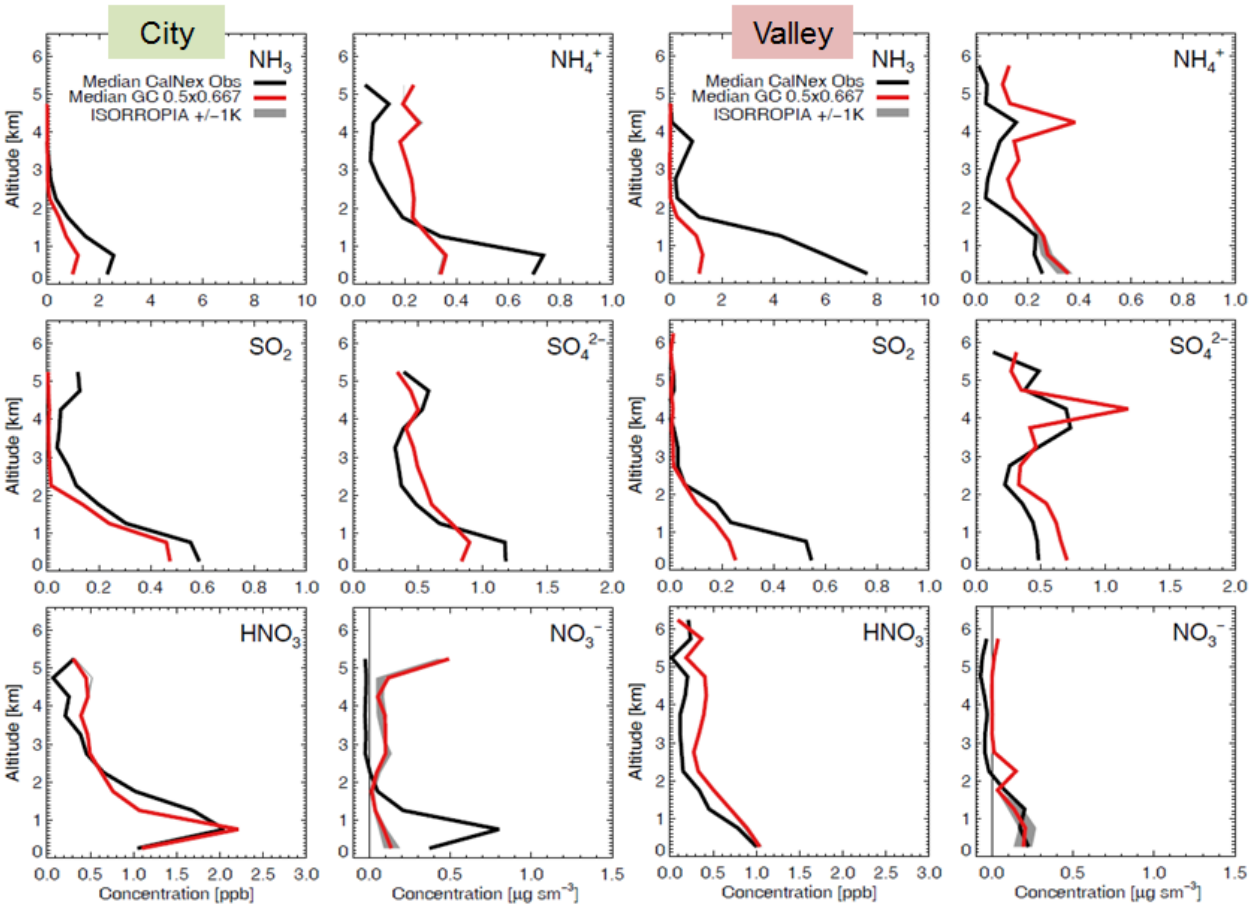

Figure 4.10: The same as Figure 4.7, but with shaded regions of +/- 1 °C variation input into ISOROPPIA II added.

significantly impact the gas-to-particle partitioning in the model such that it accounts for model bias in the inorganic aerosol system discussed in Section 4.1.

In order to examine the effects any bias in seasalt may have on partitioning in ISORROPIA II, a sensitivity simulation is run which essentially removes all Na^+ and Cl^- from the system. This simulation does not produce any significant changes in the partitioning of the system near the surface, indicating Na^+ and Cl^- concentrations in California are not large enough to significantly displace HNO_3, which would create additional NO_3^- aerosol. Since NH_3 would react with HCl instead of HNO_3 if this displacement did occur, NH_3 and NH_4^+ concentrations remain the same, as would be expected in either case. Further exploration regarding sensitivity of the system under different seasalt and RH levels remain to be conducted. Note that ISORROPIA

does not include coarse seasalt in its simulations, so any possible sink of HNO_3 onto coarse seasalt is not represented here.

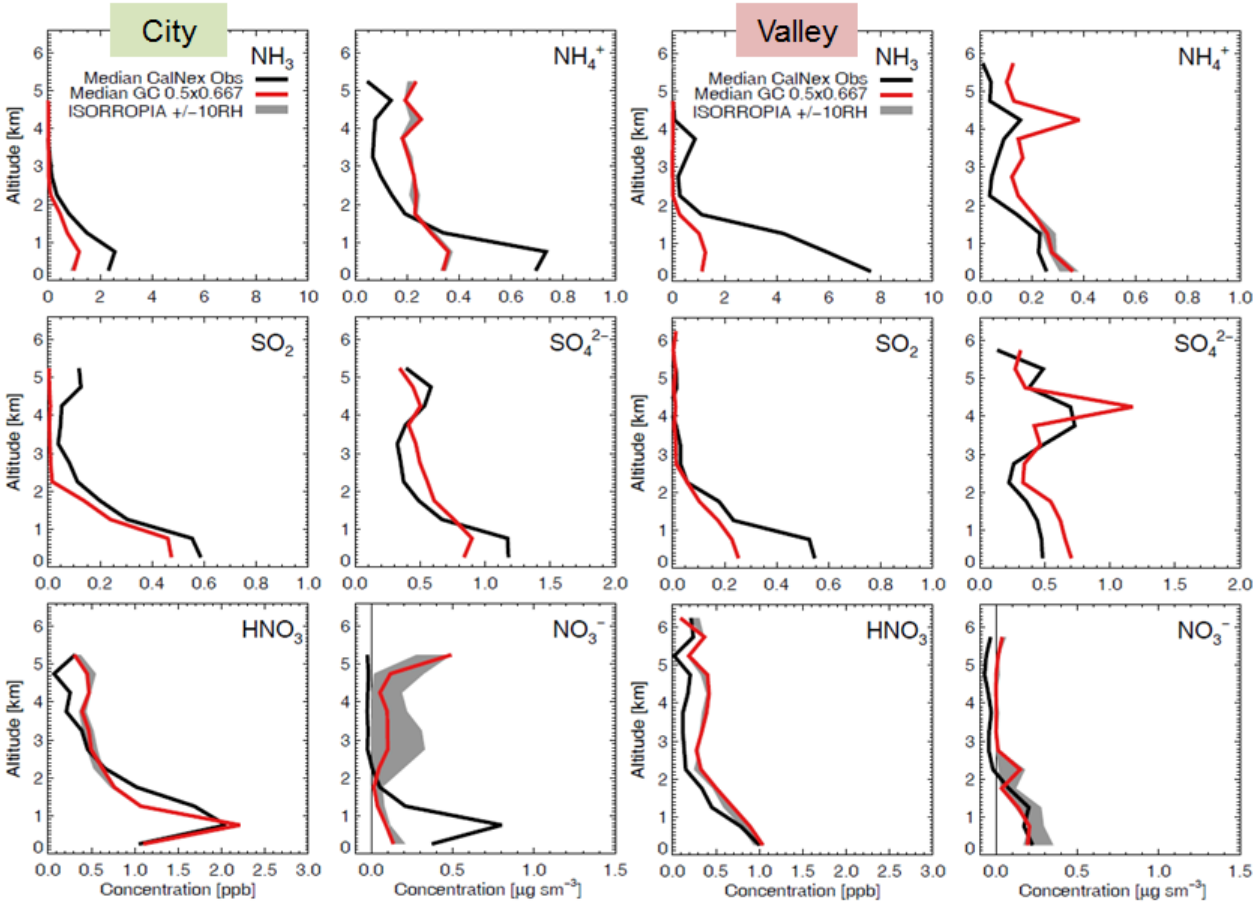

Figure 4.11: The same as Figure 4.7, but with shaded regions of +/- 10 % RH variation input into ISOROPPIA II added.

Neutralization of other atmospheric acids, such as oxalic acid, may also play a role in the system. These processes are not currently well understood. *Lefer and Talbot* [2001] report size distribution observations consistent with ammonium oxalate aerosol formation from precursor gases. Also, *Martinelango et al.* [2007] note correlations in their observations between NH_4^+ and oxalate at night, which may suggest aerosol partitioning. Measurements made during the 2002 Yosemite Aerosol Characterization Study show the presence of both $PM_{2.5}$ oxalate and oxalic acid during the summer in the Yosemite region, east of the CalNex study area [*Engling et al.*, 2006]. However, simulation of atmospheric oxalate formation by *Myriokefalitakis et al.* [2011],

which includes interactions with NH_3 and NH_4^+, shows low oxalate surface concentrations over most of California in the summer. In-situ observations have also shown that ammonium salts can accumulate on fine dust particles [*Jordan et al.*, 2003; *Sullivan et al.*, 2007], which creates additional acid removal during this process. Dust levels in California, however, are generally lower than in large export areas such as the eastern coast of Asia, where such effects have been both observed and simulated [*Fairlie et al.*, 2010]. Sources of dust in the California, particularly in the SJV, include agriculture and traffic. These have been observed to be higher in the summer/dry season than in the winter/wet season [*Chow et al.*, 2003; *Vicars and Sickman*, 2011]. Simulated fine dust concentrations at the surface in GEOS-Chem average 1 μg sm^{-3} throughout the CalNex campaign area and time period. Simulated coarse dust is a bit higher, 3 μg sm^{-3}. The annual variability of simulated dust in this area peaks during the early spring and is lowest during mid-summer. While we have neglected minor acids and dust in the GEOS-Chem simulation, we do not expect either to play a dominant role in the inorganic gas-particle system or the simulation biases described here.

4.3 Wet and Dry Deposition

Wet deposition processes allow for the removal of chemical species from the atmosphere as they are incorporated into precipitation. GEOS-Chem uses wet deposition schemes by *Liu et al.* [2001] for aerosols and *Mari et al.* [2000] for gases to determine how much of a given species is removed. These schemes are driven primarily by the presence of convection and precipitation within the meteorological input parameters. The extent to which individual species are affected is determined by physical properties such as solubility and effective Henry's law constant.

Figure 4.12 compares GEOS-Chem modeled monthly mean wet and dry deposition flux of NH_x in California for May and June 2010. Over the domain shown, for May and June the NH_x dry deposition flux totals are 2.8 Gg N and 3.6 Gg N, respectively, while the NH_x wet deposition flux totals are 1.6 Gg N and 0.5 Gg N. From these totals, we see that the wet deposition flux of NH_x makes up a much smaller fraction of total deposition in California than dry deposition in the summer months. This is due to the lack of precipitation at that time. Most of the precipitation occurs over the mountains to the east of the Valley. As this is largely driven by the regional meteorology, wet deposition of SO_x and TNO_3 follow similar seasonal patterns.

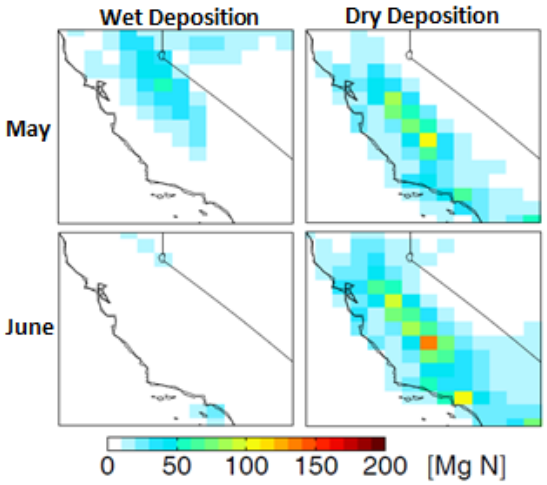

Figure 4.12: Monthly mean GEOS-Chem wet (left) and dry (right) deposition flux of NH_x over California for May (top) and June (bottom) 2010.

As the CalNex campaign did not include a specific effort to make deposition measurements, simulated wet deposition from GEOS-Chem is compared with aerosol wet deposition measurements from the National Atmospheric Deposition Program National Trends Network (NADP/NTN) (nadp.sws.uiuc.edu/ntn) sites in California to see if any clear model bias exists. Ion concentrations are measured from precipitation samples collected. Monthly mean wet deposition observations and model output at 9 NADP/NTN sites throughout 2010 are shown in

Figure 4.13. In May and June (highlighted in grey), the observations and model agree that wet deposition levels of all three aerosol species are low, both in absolute terms and compared to other times of the year. Only sites C, E and F, which are located in the mountains on the east side of the Valley, experience any appreciable wet deposition, and this is only in May. Thus, any model errors in wet deposition do not play a significant role in the discrepancies between the CalNex observations and GEOS-Chem simulation within the observed Valley or City region.

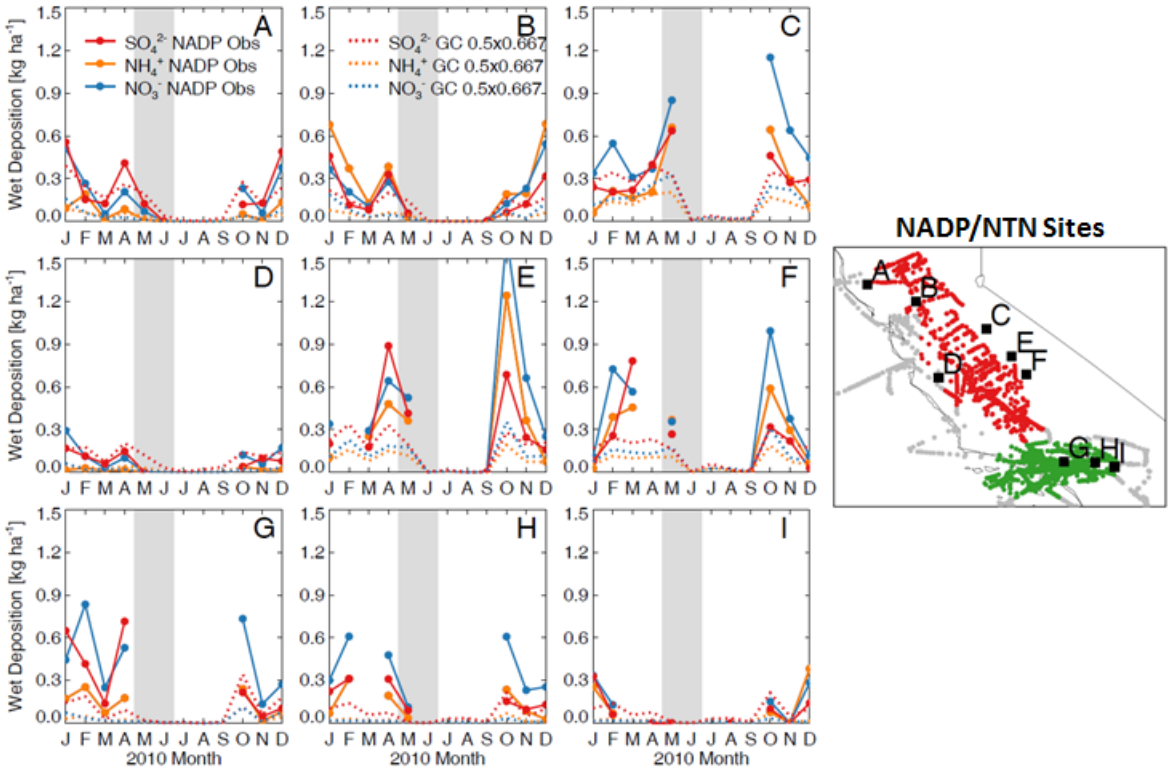

Figure 4.13: Monthly mean wet deposition of aerosol species at 9 NADP/NTN sites and GEOS-Chem output in corresponding grid boxes in California. Months without observations indicate no precipitation/sample. The period of the CalNex campaign is highlighted in grey.

GEOS-Chem uses the *Wesely* [1989] resistance parameterization for dry deposition. This scheme combines aerodynamic resistance, boundary layer resistance and canopy surface resistance terms to calculate a deposition velocity. This deposition velocity is combined with the ambient species concentration to determine the dry deposition flux. Resistances themselves are calculated from a combination of meteorological parameters such as temperature and incident

solar radiation, atmospheric stability, land surface type and species specific parameters such as molecular weight and Henry's law constant. Aerosol species resistances take into account the size of the aerosol, rather than individual species characteristics.

Figure 4.14 shows the spatial and inter-species variation of the dry deposition velocities calculated by GEOS-Chem over California for May 2010. Velocities are generally higher over the ocean, assumed to be a smooth surface. Velocities are also higher for HNO_3 than NH_3 and SO_2 (which are similar) due to nitric acid's much higher Henry's law constant. The dry deposition velocity is the same for all three aerosol species. On land, spatial variation is highlighted by peak deposition velocity areas, such as the Valley region for NH_3 and SO_2, northern California for HNO_3 and the mountains west of the Valley for the aerosol species. This on-land variation for each species reflects the assumed vegetation type(s) in each grid box.

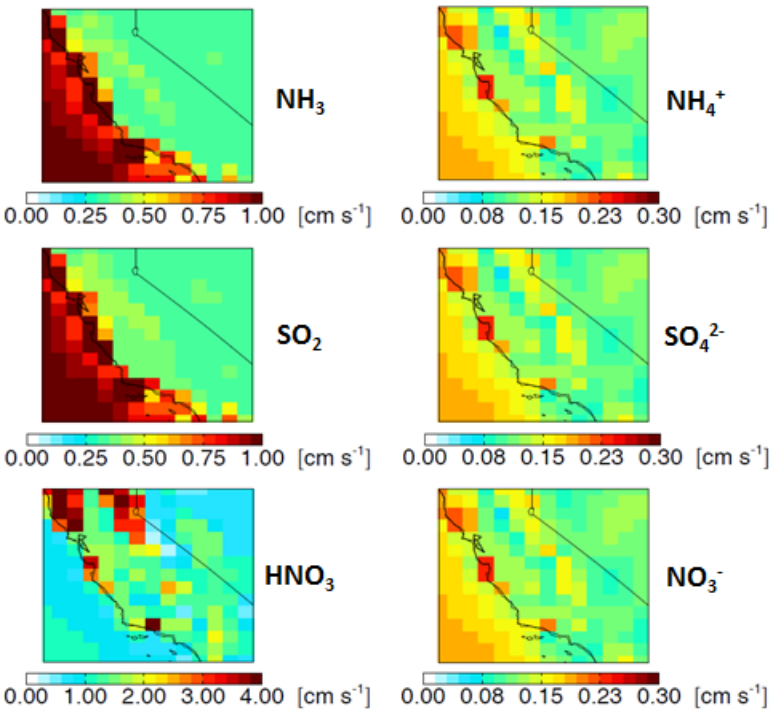

Figure 4.14: Monthly mean GEOS-Chem calculated dry deposition velocity for May 2010 over California.

Average dry deposition velocity values from 7 California sites in the EPA Clean Air Status and Trends Network (CASTNET) (www.epa.gov/castnet) in May and June 2007 - 2009 are compared with GEOS-Chem output for May and June 2010 in Figure 4.15. CASTNET data for 2010 are not available, nor does CASTNET report NH_3 dry deposition velocities. It is critical to note that the dry deposition velocities from CASTNET are derived quantities from the Multi-Layer Model (MLM) based on measured meteorology parameters, including temperature, wind velocity, humidity and solar radiation. Thus, the comparison with GEOS-Chem is in fact a

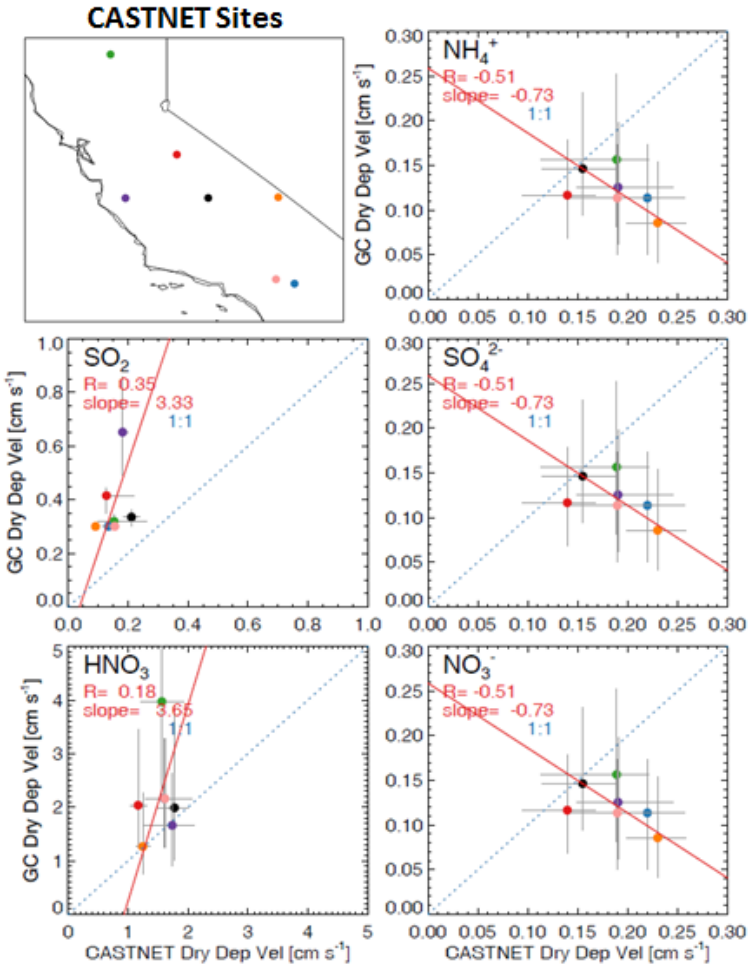

Figure 4.15: Scatterplots of mean CASTNET and GEOS-Chem dry deposition velocity at 7 sites in California. CASTNET data are weekly May-June 2007-2009 values, and GEOS-Chem output is daily for May-June 2010. Linear regression line is shown in red, 1:1 slope line shown in blue and grey lines represent extent of minimum and maximum velocity values. NH_3 deposition is not measured by CASTNET.

comparison of two models. However we use these comparisons to provide an estimate of potential bias in the GEOS-Chem simulation. Based on these few point sites for comparison, the model deposition velocity is biased high for SO_2 and a bit low for the aerosols. The HNO_3 comparison is reasonable.

A sensitivity simulation is conducted where the dry deposition velocity biases in the model are decreased by altering the previously-calculated velocity in the dry deposition module. SO_2 dry deposition velocity is reduced by 50 %, lowering the minimum velocity from 0.3 cm s^{-1} to 0.2 cm s^{-1}. Aerosol dry deposition velocity is increased by 70 %, as suggested by the discrepancies shown in Figure 4.15. Figure 4.16 shows the results of this simulation by

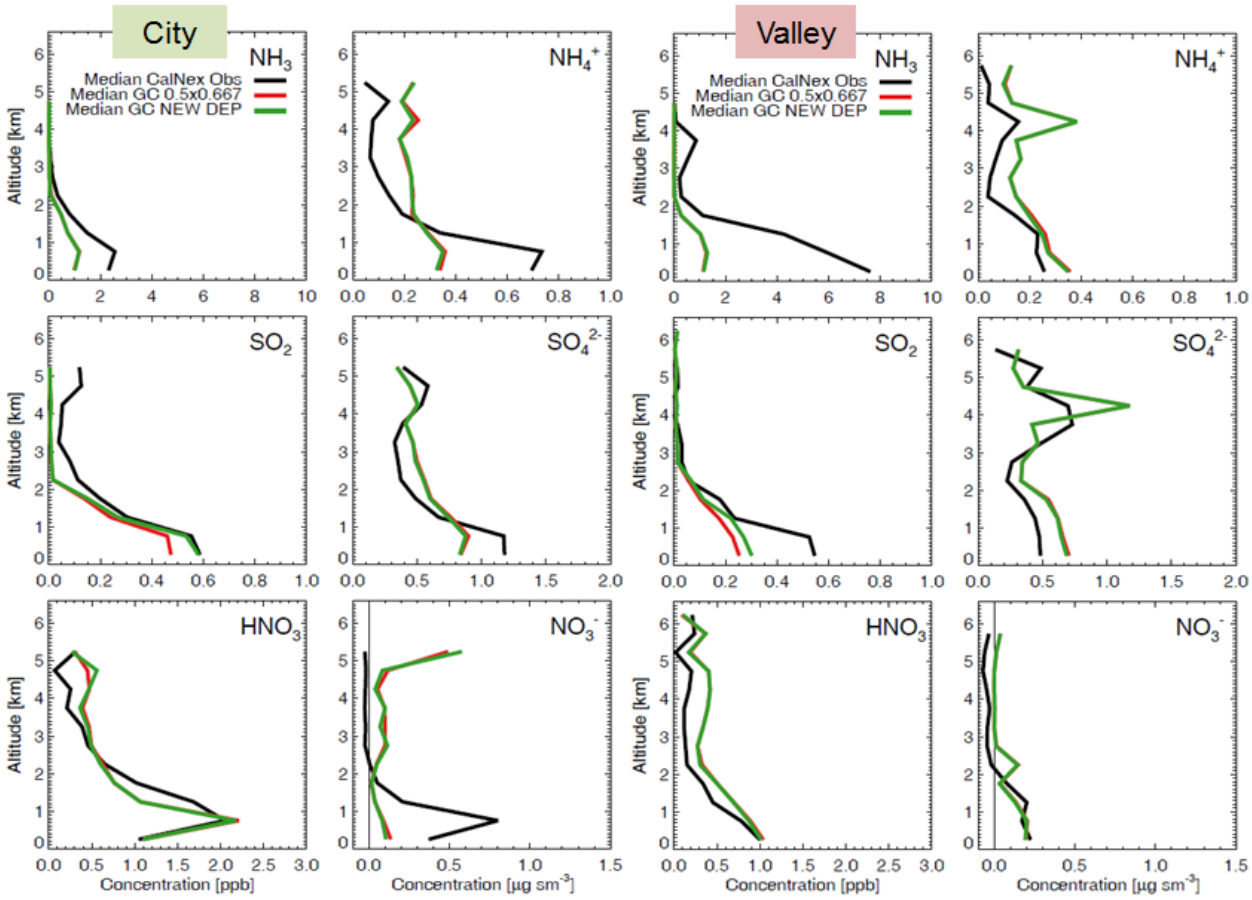

Figure 4.16: Same as Figure 4.7, but with vertical profiles resulting from the dry deposition sensitivity simulation added in green.

comparing the baseline median vertical profiles simulated with this new sensitivity simulation (split into the City and Valley regions). The impacts of these changes are small. Near-surface SO_2 in the City is increased enough to eliminate the model bias in this region. A similar increase is seen in the Valley, but it is only a small part of the difference between the observations and simulation. The aerosol concentrations in both regions decrease only very slightly. While the improvement in surface SO_2 concentration in the City made by altering the SO_2 dry deposition velocity does correct the original discrepancy, given the potential bias due to the modeled nature of the CASTNET values, corrections made to the GEOS-Chem model bias may not be entirely warranted. Furthermore, the relative insensitivity of the simulation to the assumed dry deposition velocities suggests that this is not a major source of bias in the model simulation. We note that the dry deposition velocities of ammonia have not been evaluated against observations, although a similar 50 % decrease in simulated NH_3 dry deposition velocity does not produce any significant changes to the species concentrations.

As mentioned above, Figure 4.12 shows that a majority of the NH_x mass loss to deposition in California during May and June is via dry processes. Splitting NH_x into its components, as in Figure 4.17, nearly all of this is dry deposition of gaseous NH_3 rather than NH_4^+ aerosol. Similarly for SO_x (not shown) and TNO_3, the dry deposition of the gas species dominates that of the aerosol. This explains the small change in aerosol concentration when the dry deposition velocity was increased by 70 %. Dry deposition of HNO_3 clearly dominates the total nitrogen (N) deposition throughout California. This is generally higher in June than in May. NH_3 deposition is higher in the Valley than in the City, as expected given the differences in emissions. The sum of City and Valley total N deposition does not make up the total California

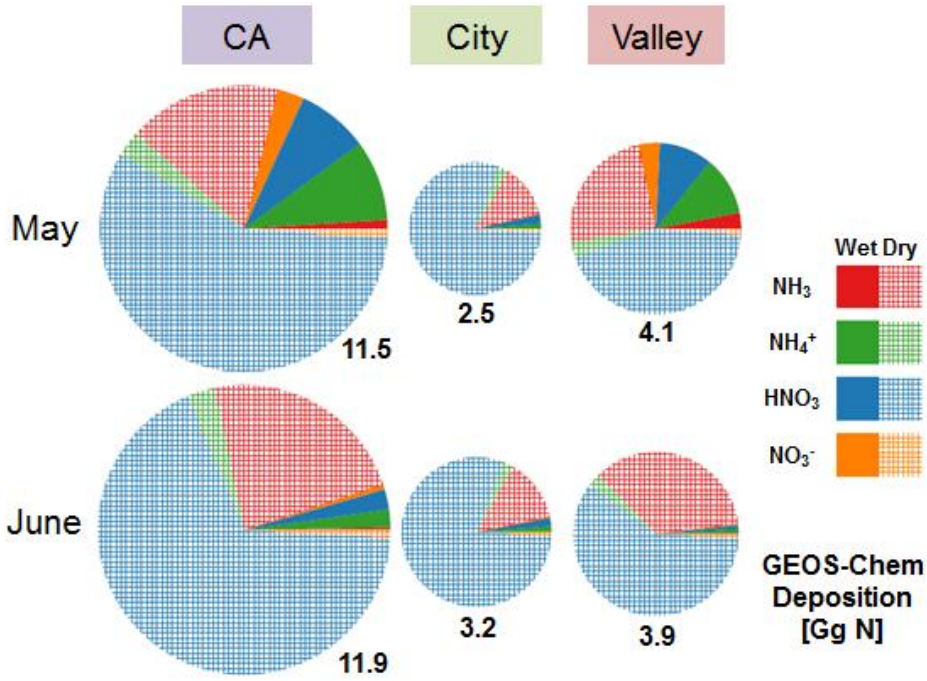

Figure 4.17: Comparison of standard GEOS-Chem N deposition by type, species, region and month. Top row is May, while bottom row is June. Left column is area of California (CA) contained in the square domain in Figure 4.13. Middle column is City and right column is Valley as defined above. Species are NH_3 (red), NH_4^+ (green), HNO_3 (blue), NO_3^- (orange). Wet deposition is solid color; dry deposition is pattern-filled.

N deposition in either month due to deposition which occurs away from these high emissions regions.

Comparing the N deposition in California with results from *Zhang et al.* [2012] shows that wet deposition makes up a much larger portion (about 40 %) of N deposition over the entire United States. This is an annual value, however, and California does experience higher wet deposition rates during the winter. As in California, HNO_3 dry deposition is the largest N deposition source over the entire United States, and the gas phase dominates dry deposition flux.

4.4 Emissions

The emissions of NH_3, SO_x and NO_x into GEOS-Chem are specified according to inventories, which attempt to quantify chemical species released into the atmosphere by source

and location. The largest source of these species over California is from anthropogenic activity (see Section 3.2). In GEOS-Chem, anthropogenic emissions are given by the NEI-2005, which is based on information from 1999 - 2005. Given the rapid growth of human and livestock populations in parts of California [United States Department of Agriculture California livestock inventory (www.nass.usda.gov/ca)], errors may exist within this inventory for the time of our study period in 2010. Also, the nature of gas species, especially NH_3, make measurements difficult and under-reporting may occur as a result.

We investigate whether adjusting anthropogenic emissions from NEI-2005 in a manner consistent with the biases in Figures 4.6 and 4.7 can reconcile our model simulation with the CalNex observations. Our initial comparisons showed that the model NH_3 concentrations were low in both regions, but this difference is much greater in the Valley. A uniform increase in anthropogenic NH_3 emission over the entire domain would not provide insight into the incorrect inventory source or differentiate between NH_3 sources in the two regions. Instead, we are able to split the NEI-2005 NH_3 emissions into several source sectors, including livestock and mobile sources. Figure 4.18 compares the total NEI-2005 NH_3 emissions over California with the NH_3

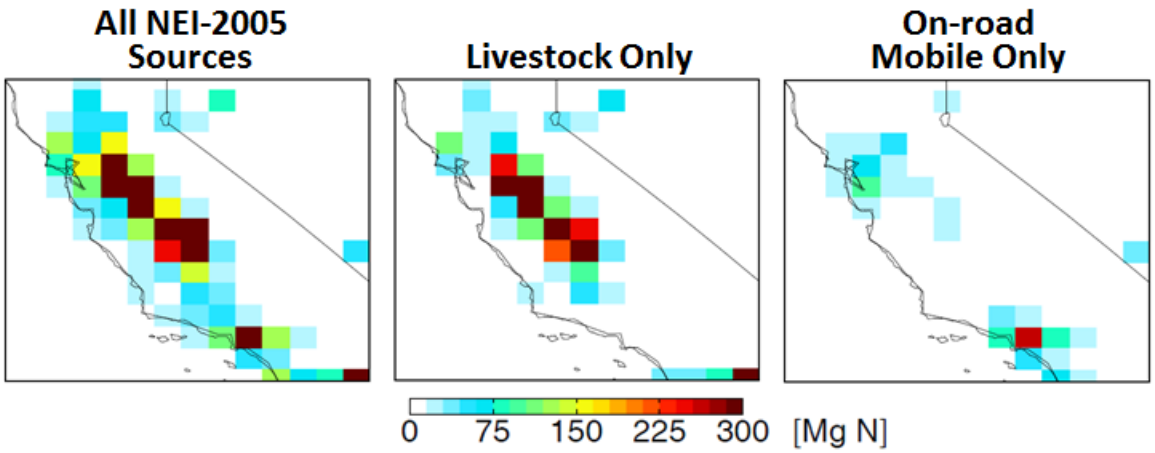

Figure 4.18: NEI-2005 NH_3 emissions in GEOS-Chem for May 2010 over California: all sources (left), livestock only (center) and on-road mobile only (right).

from only livestock and on-road mobile sources, for May. This clearly shows the livestock NH_3 emission in the Valley region and the on-road mobile NH_3 source in the City region, as well as in the vicinity of San Francisco. Isolated on-road mobile sources in the Valley represent cities such as Fresno and Bakersfield as well as traffic on Interstate-5. We investigate the impact of increasing the livestock NH_3 emission by a factor of 5 over the entire inventory area in our modified simulation.

Using the same CalNex plane flight measurements as in this study, *Nowak et al.* [2012] show that the NEI-2005 NH_3 emissions are quite low for the eastern side of the LA Basin, where many dairy operations exist. They report a measured NH_3 emission rate of 12 - 64 Gg yr^{-1} from livestock in this eastern LA region, compared to the NEI-2005 rate of about 0.37 Gg yr^{-1}. This emission rate is calculated from the NH_3 mixing ratio enhancements measured during the crosswind flight transects over eastern LA integrated with the wind speed and mixing height. The population of cattle in this area was about 298,000 in 2010. We set the livestock NH_3 emission rate in the single east LA model gridbox consistent with the region discussed by *Nowak et al.* [2012] to 12 Gg yr^{-1} in our modified simulation. This is more than 30 times the original value, rather than 5 times increase imposed elsewhere.

The model SO_2 concentrations are underestimated in the Valley as well. This low bias is larger in the southern Valley region than in the north. In an effort to correct this, we increase the northern and southern Valley SO_2 emission by 3 times and 10 times, respectively, in our modified simulation. This increase may be the result of greater need for electricity generation or oil refining in the region, however the scaling factors selected are somewhat arbitrary and based on the observed bias in the baseline simulation. The emission rates for both anthropogenic NH_3 and SO_x in the standard and modified GEOS-Chem simulations are shown in Figure 4.19.

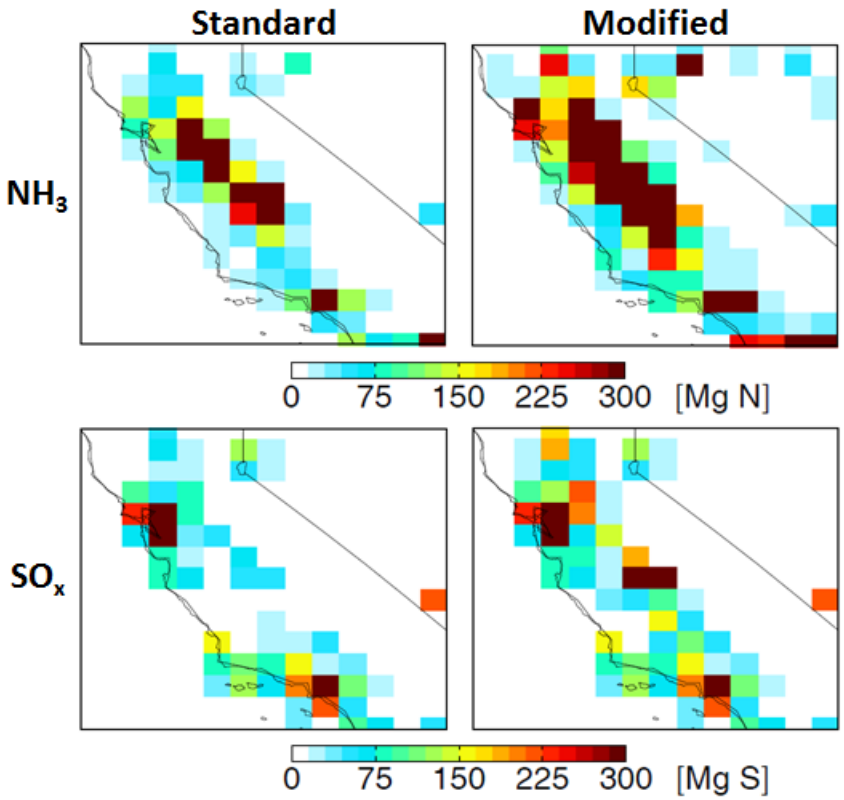

Figure 4.19: Anthropogenic NH_3 (top) and SO_x (bottom) emissions in GEOS-Chem for May 2010 over California: standard simulation (left), modified simulation (right).

Vertical profiles comparing the results from the modified emissions simulation with the standard run are shown in Figure 4.20. As changes in surface emissions were made, most median concentration differences are most pronounced in the surface layer. In the City region, the low NH_3 concentration bias is more than made up for by the increased emissions. However the increase in emissions compensates for only about two-thirds of the bias in NH_3 in the Valley, with a pronounced near-surface underestimate. This could be due to errors in the calculation of the boundary layer or lack of surface NH_3 re-emission from a bi-directional flux (see Chapter 6). The low bias in SO_2 concentrations in both regions are eliminated. Reaction with increased NH_3 emission in the Valley decreases the median HNO_3 concentrations in that region slightly to correct the small over-prediction in the standard simulation. HNO_3 in the City remains the same,

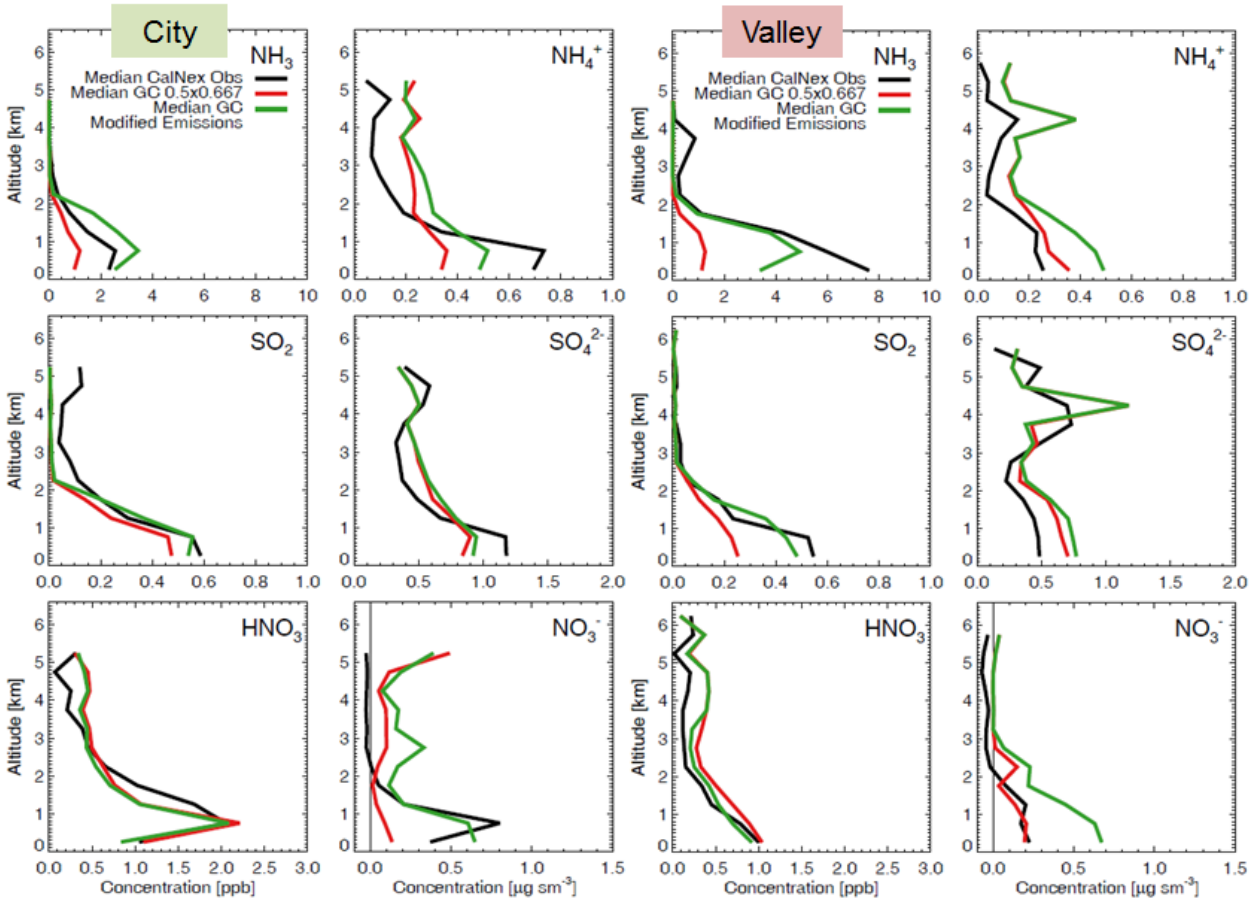

Figure 4.20: Same as Figure 4.7, but with vertical profiles resulting from the GEOS-Chem simulation with modified emissions added in green.

in good agreement with observations. The aerosol species increase in both regions due to increased availability of NH_3 and SO_2. In the case of NH_4^+ and SO_4^{2-}, this worsens the already high-biased comparison in the Valley, but slightly improves the simulation in the City. The large increase in NO_3^- concentration brings the comparison in the City into agreement near the surface and creates a high bias in the Valley. Gridded comparisons, shown in Figure 4.21, generally support these changes in concentration from the modified emissions simulation. The low bias which remains in NH_3 and SO_2 concentrations is isolated more toward the southern Valley. Over-prediction in the aerosol concentration occurs largely in the northern Valley. This is especially true for NO_3^-.

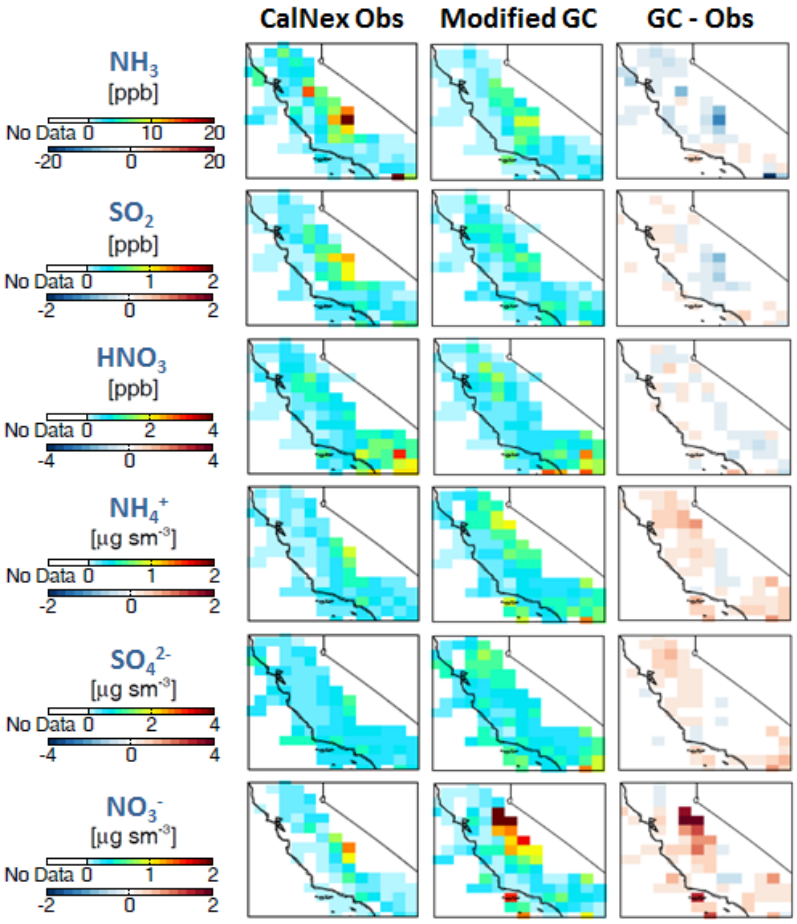

Figure 4.21: Same as Figure 4.6, but for modified emissions GEOS-Chem simulation.

The results of these emissions modifications suggest that uncertainties in the GEOS-Chem simulation of the inorganic gas-particle system are dominated by emissions. Accurate emissions inventories are critical to the ability to accurately model reactive nitrogen and PM formation in California. The emissions modifications we have made are the largest source of concentration variation and the closest we have come to reducing initial errors among the factors examined in Chapter 4.

However, we note that the diurnal NH_3 emission is currently constant in GEOS-Chem. This is not realistic as NH_3 emission via volatilization increases during midday when ambient temperatures are higher. Replicating this diurnal variation through re-distribution of total daily NH_3 emission may help simulating the large NH_3 concentrations observed during CalNex.

However, the limited characterization of the diurnal profile from the CalNex aircraft measurements makes it challenging to evaluate any such emission modification. Additional directions for further improvements and investigation are discussed in Chapter 6.

5. Applications

5.1 PM Formation

Understanding the formation of inorganic particulate matter in California is important to diagnose and predict air quality and visibility issues in this high-emission region. We have established that emissions can be a large source of inaccuracies in GEOS-Chem when compared with in-situ observations. Figure 5.1 summarizes the surface air quality and PM composition for our two regions in California. In particular, it compares the CalNex airborne observations with the standard GEOS-Chem simulation and the results due to anthropogenic emissions modifications in this study. The CalNex observations show that inorganic PM concentrations are about 3 times as high in the City as in the Valley below 1 km, with median concentrations of

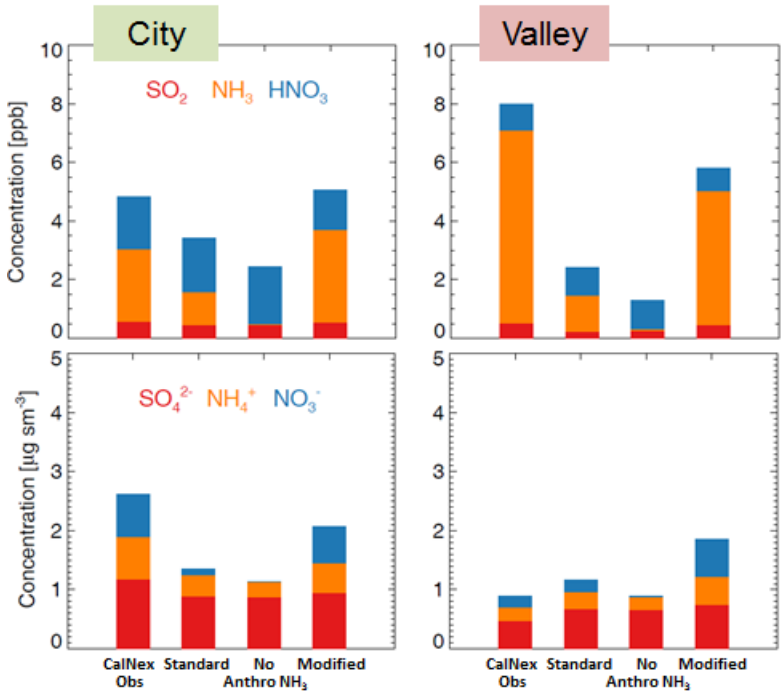

Figure 5.1: Median species concentrations below 1 km. Comparing gases species (top) with aerosol species (bottom), City region (left) with Valley region (right) for four cases: CalNex plane flight observations, standard GEOS-Chem simulation, simulation with no anthropogenic NH3 and modified simulation with increased emissions.

2.62 and 0.90 μg sm^{-3}, respectively. Sulfate makes up 45 % of observed inorganic PM mass in the City and 53 % in the Valley, while nitrate makes up 28 % and 21 % in those regions.

It is clear that anthropogenic NH_3 emissions are vital to the production of NO_3^- in both regions. If we run a simulation with anthropogenic NH_3 emissions set to zero, this removes a large portion of the atmospheric base required for creation of inorganic aerosol. Results from this simulation indicate that all NH_3 has been converted into NH_4^+ through the reaction with acids. SO_2 and SO_4^{2-} concentrations are unaffected, but SO_4^{2-} is present in more acidic form with the reduced neutralization potential from NH_3. Any remaining NH_3 would react with HNO_3 to from equilibrium with NH_4NO_3, but NO_3^- concentrations are zero in both regions suggesting that emitted NH_3 in this scenario is entirely consumed through neutralization of H_2SO_4.

Increasing NH_3 and SO_2 emissions as described in the modified simulation decreases the overall extent of bias seen in the initial comparison of the observations to standard GEOS-Chem. This modified simulation yields median inorganic PM concentrations of 2.06 μg sm^{-3} in the City and 1.86 μg sm^{-3} in the Valley. Comparison of gas species is improved or consistent with the initial comparisons in both regions. Aerosol concentrations in the City are also greatly improved, especially for NH_4^+ and NO_3^-. The largest remaining issue is in the simulated Valley aerosol concentrations, which are initially too high (by 30 %), compared to the observations, and are increased further with the modified emissions (now 107 % overestimate). This occurs, despite the continued underestimate of the gas-phase precursors in the same region of 22 %. Possible causes of this over-prediction include a missing loss-mechanism, insufficient ventilation or poor representation of transport and export from the Valley due to insufficiently resolved terrain. Increasing aerosol dry deposition velocity was shown to be ineffective above. Further investigation is required to improve the PM simulation in this challenging region.

Many studies of the LA Basin have observed the formation of NH_4NO_3 downwind of LA as the NO_x emitted from the city reacts with large amounts of NH_3 from farms to the east of LA. Up until now, for simplicity, we have not isolated the LA Basin (contained within the City region) which consists of roughly 2 gridboxes in the 0.5° x 0.667° resolution model. However, Figure 5.2 shows that the two gridboxes, one for LA and one for east of LA, do indeed present very different regimes of emissions and PM formation. More than 400 measurements still fall within each gridbox. Observed inorganic PM in East LA is 20 % higher than in LA and is made up of 44 % NO_3^- compared to 33 % in LA. Figure 5.2 also shows the results of a model simulation based on a study by *Bishop et al.* [2010], which finds that NH_3 emissions have increased in LA at the cost of NO_x emissions, based on changing driving habits and the increasing use of catalytic conversion. In our "mobile" simulation, we double the emissions of

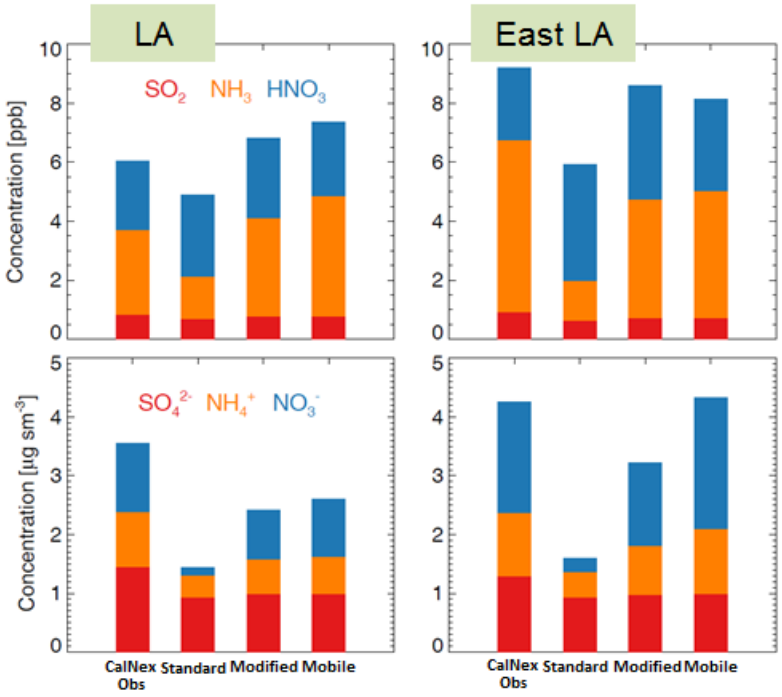

Figure 5.2: Median species concentrations below 1 km. Comparing gases species (top) with aerosol species (bottom), LA gridbox (left) with East LA gridbox (right) for four cases: CalNex airborne observations, standard GEOS-Chem simulation, modified simulation with increased emissions and simulation with mobile nitrogen emissions modifications.

on-road mobile NH_3 in the City and decrease NO_x emissions by equal moles of N. These emissions changes are in addition to those made in the modified simulation.

In both boxes, for all species, the modified emissions simulation is an improvement over the standard GEOS-Chem simulation. The modified simulation clearly captures the increased NH_4NO_3 concentration in East LA, although the NH_3 and HNO_3 concentration are greater here than in LA as well. As SO_4^{2-} is unchanged, total inorganic PM from the modified simulation is also greater in East LA than in LA. Comparing the results of the mobile simulation to those of the modified simulation, there is a larger increase in the NH_4NO_3 concentration in East LA than in LA. This demonstrates the strong impact of upwind emissions (on-road mobile NH_3 emissions increase and the corresponding NO_x decrease is larger in the LA box) on the downwind PM formation in East LA. It suggests that providing an additional NH_3 source in LA can lead to significant down-wind production of NH_4NO_3 due to the excess availability of HNO_3 in the city. Both the modified and mobile simulations provide a better alternative to the standard GEOS-Chem version, with the mobile source simulation providing a near-perfect simulation of East LA PM.

Given the general improvements made by the modified emissions GEOS-Chem simulation, we can investigate the implications for PM formation in California outside of the CalNex period used for this evaluation. Figure 5.3 compares mean concentrations in the lowest 1 km in the same City and Valley regions during June and December 2010. We use mean in this case as the concentrations are already averaged over the entire month in each gridbox, and only simulated concentrations are shown, thus there is no need to account for unresolved plumes. In each region, the model simulates similar PM behavior changes between June and December across all simulations. In the City, mean inorganic PM concentration is 1.86 μg sm^{-3} greater in

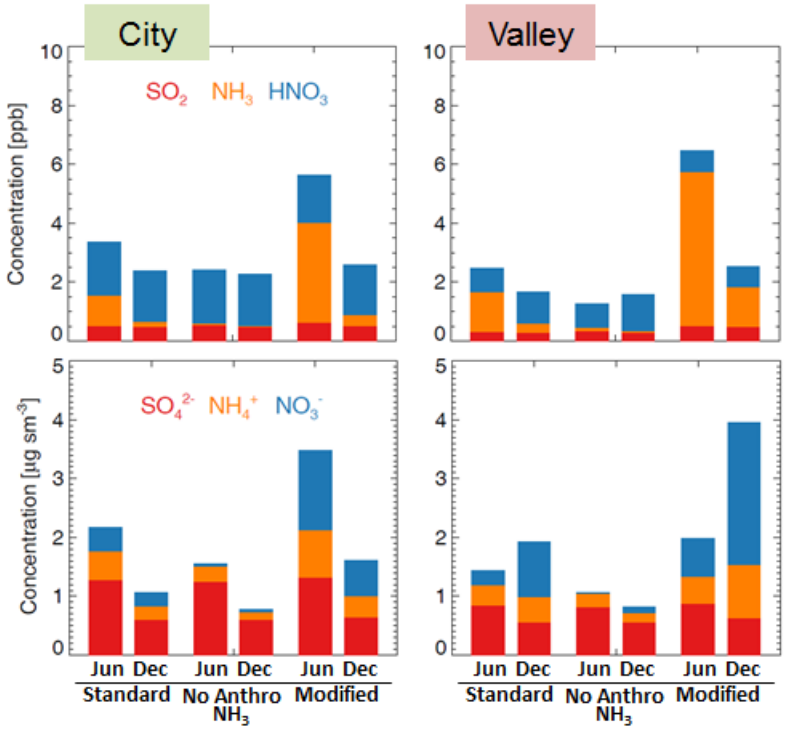

Figure 5.3: Mean species concentrations in the lowest 1 km for June and December 2010. Comparing gases species (top) with aerosol species (bottom), City region (left) with Valley region (right) for three cases: standard GEOS-Chem simulation, simulation with no anthropogenic NH_3 and modified simulation with increased emissions.

June than in December. This is likely due to decreased anthropogenic NH_3 emissions in December, which causes NH_3 to be limited and reduces NH_4NO_3 formation despite high HNO_3 availability. Sulfate concentration is also lower in December, likely due to slower SO_2 oxidation during the winter despite similar SO_2 availability. There is a mean decrease in simulated planetary boundary layer (PBL) height in the City region from 1.2 km in June to 0.7 km in December. This may slightly increase PM concentrations near the surface from what they would be due to only the seasonal effects which decrease PM formation as described above.

In the Valley, aerosol concentrations are double in December compared to June. Even though the anthropogenic NH_3 decreases by the same proportion as in the City, there is still abundant NH_3 available for reaction. The large increase in NH_4NO_3 in December is due to colder wintertime temperatures which shift the equilibrium partitioning toward favoring the aerosol

rather than gas phase. Nitrate shifts from composing 32 % of Valley inorganic PM in June to 61 % in December. A secondary cause may be an increase in inversion events during the winter, which may trap pollutants in the Valley region. The mean simulated PBL height in this region does decrease from 1.7 km in June to 0.7 km in December; however, accurately simulating the timescales of this trapping in the model may be difficult. The same effect on SO_4^{2-} is simulated in the Valley as well, where SO_4^{2-} is lower in the winter due to slower SO_2 oxidation. Frequent winter cloud and fog activity in the Valley can also accelerate the deposition of PM species during this time. This removal counters the increase in SO_4^{+} production which occurs when more water is available. Given the very different behavior in the Valley in December, it would be useful to evaluate the model using observations during this time as well.

5.2 Export of Excess NH_3

Ammonia which is not partitioned into aerosol or deposited near its emission region can be transported, given the proper meteorological conditions, and react or be deposited elsewhere. This excess NH_3 often occurs due to the very large emission rates in certain areas. Figure 5.4 suggests that the Valley region in California is one such region, as there is a positive net NH_x

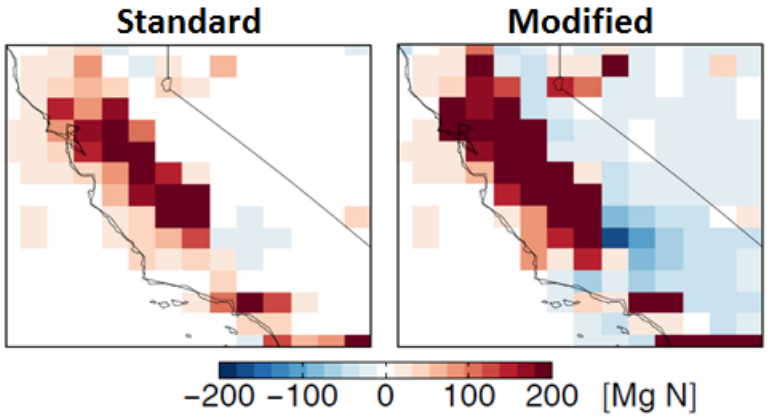

Figure 5.4: June 2010 net NH_x flux (emission – deposition) over California for standard and modified GEOS-Chem simulations.

flux (emission – deposition) here. Negative net NH_x flux occurs at the southern end of the Valley, where deposition dominates. This down-wind deposition is enhanced in the modified simulation where increased NH_3 emissions in the Valley lead to enhanced export from the region.

Further evidence of export of excess NH_3 out of the Valley is given by Figure 5.5, which shows NH_3 surface and column concentrations in California and vertical profiles of NH_3 for three regions: the City, Valley and an East export region. We compare June and December 2010 using the modified simulation. Export of NH_3 out of the southern end of the Valley region is evident during June. Column concentrations are high in this southeastern area and the vertical profile of the East region is similar to that of City, even though there is very little NH_3 emission in this area. Export from the Valley may even be contributing to NH_3 concentrations aloft in the City region (as suggested by the column concentrations), which we had largely assumed to be separated from the Valley region in our analysis. In December, this export does not occur. In the wintertime, lower NH_3 levels are efficiently partitioned into NH_4NO_3 under cooler conditions,

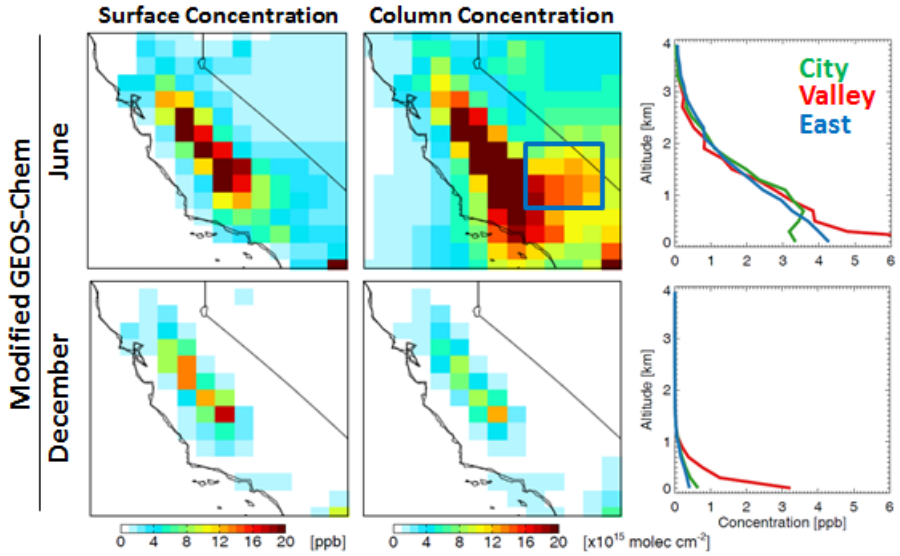

Figure 5.5: Ammonia surface and column concentrations in California; vertical profiles of City (green), Valley (red) and East (blue) regions for June and December 2010 during the modified simulation with increased emissions. The blue box represents the area of the East region.

leaving little to no excess NH_3 to be exported from the region.

The NH_3 export shown to the East region in the model cannot be evaluated using CalNex observations, as the campaign did not make measurements there. An alternative to in-situ measurements is the use of space-based remote sensing to observe concentrations of NH_3. The IASI instrument can be used to gather such values [*Clarisse et al.*, 2010]. Figure 5.6 shows the average IASI retrieved column concentration for June, July and August 2009 over California (observations for 2010 are not available). The satellite measurements qualitatively confirm the high NH_3 concentration in the Valley region and the export of NH_3 out of the southern Valley.

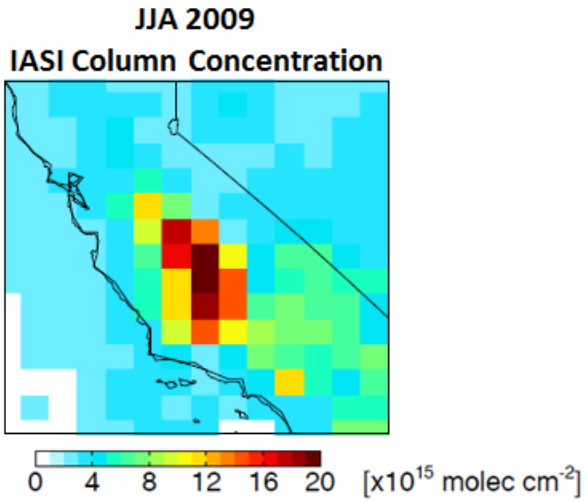

Figure 5.6: Average summer (June, July, August) 2009 IASI-retrieved NH_3 column concentrations over California [*Clarisse et al.*, 2010].

The effects of summertime NH_3 export on air quality downwind can be seen in Figure 5.7, where we plot the mean surface concentrations of NH_4^+ in California for June 2010 using the modified simulation. This represents the distribution of inorganic PM from both $(NH_4)_2SO_4$ and NH_4NO_3 in the region. An obvious hotspot exists in the City region, where a mean NH_4^+ concentration of 1.44 µg sm^{-3} is simulated. These high concentrations are primarily due to local sources of both NH_3 and NO_x, although it is possible some enhancement is occurring from NH_3 exported southward from the Valley as seen aloft in Figure 5.5. NH_4^+ concentrations are lower in

the Valley and East export region, 0.69 and 0.34 µg sm^{-3}, respectively. Figure 5.7 shows that the conversion of localized NH_3 sources in the Valley enhances NH_4^+ concentrations regionally. However, given the available ammonia, NH_4^+ formation in the region is modest, likely limited by the supply of acidic gases (as well as warm temperatures favoring the gas-phase). This suggests that the potential exists for further PM formation and export if emissions of SO_2 and NO_x increase.

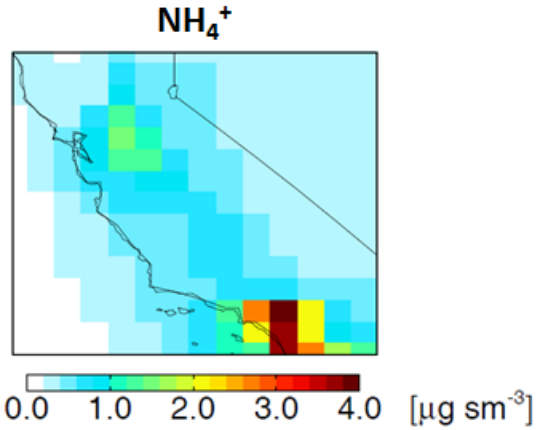

Figure 5.7: Mean NH_4^+ surface concentration in California for June 2010 from the modified simulation with increased emissions.

6. Conclusions and Future Work

We have evaluated the representation of the ammonia and inorganic aerosol system in the GEOS-Chem chemical transport model using aircraft observations from the CalNex campaign in May and June 2010. Initial comparisons of observations with the simulation show under-prediction of NH_3 and SO_2 in two regions in California, near LA and the Central Valley. Median concentrations of NH_4^+, SO_4^{2-} and NO_3^- are under-predicted near LA as well, but NH_4^+ and SO_4^{2-} are over-predicted in the Valley.

Sensitivity analysis of several processes within the model indicates that emissions provide the best solution for simulation modification in order to account for discrepancies with observations. Increasing anthropogenic emissions of NH_3 and SO_2 increases the concentrations of those gases as well as inorganic PM formation in both regions. This reduces the initial model bias in all species, except aerosols in the Valley. This suggests that the NEI-2005 emission inventory does not adequately describe both livestock NH_3 throughout California and anthropogenic SO_2 sources in the Valley.

Using the modified emissions simulation, which increased NH_3 from livestock and SO_2, we assess inorganic PM and related air quality in each region during June and December. June PM concentrations are higher near LA than in the Valley, and NO_3^- provides a larger portion of the PM near LA. This is reversed in December, when NH_3 emissions decrease and colder temperatures favor NH_4NO_3 formation. Valley PM concentrations are twice as high during this time than in June.

Higher emissions and warmer temperatures favor export of excess NH_3 out of the Valley in summertime. In addition to deposition of this NH_3 in the export regions, which causes environmental degradation, inorganic PM is formed in limited amounts. The remaining reservoir

of NH_3 in the Valley indicates that this formation and the associated air quality degradation could dramatically increase should the emissions of atmospheric acids increase. This seems possible given current projections of SJV human population: about 20 % increase over 2010 population by 2020 and 60 % increase by 2040 [*State of California*, 2012]. However, advances in emissions technology and implementation may counteract some or all of the effects of population growth [*Steiner et al.*, 2006].

Satellite retrievals of NH_3 by instruments such as the Tropospheric Emission Spectrometer (TES) [*Beer et al.*, 2008] and the Infrared Atmospheric Sounding Interferometer (IASI) [*Clarisse et al.*, 2009] have been developed relatively recently. These space-based observations are useful in areas where no in-situ observations are available and can be implemented on regional scales to assist ground-based networks. There are currently challenges with retrieval sensitivity, but looking at long-term and multi-year averages could be a good complement to specific field campaigns such as CalNex. Figure 5.6 shows a preliminary snapshot of satellite observations of ammonia in California. Future work will use the temporal trends in these observations to further investigate the seasonality of emissions in different regions in California.

The current version of GEOS-Chem does not include any parameterization of a bi-directional NH_3 flux, which refers to the ability of plants to both absorb and emit NH_3. The direction of this flux depends on comparing the ambient NH_3 concentration to a certain compensation point [*Farquhar et al.*, 1980]. Resistance models, similar to the dry deposition scheme currently in GEOS-Chem, have been developed to derive this compensation point based on meteorology and plant types at a given time and place [*Flechard et al.*, 1999; *Nemitz et al.*, 2001]. Inclusion of bi-directional NH_3 flux in chemical transport models should improve their

performance by accounting for the day-to-day re-emission of NH_3 back into the atmosphere based on the variability of meteorological conditions, which is currently not included [*Zhang et al.*, 2010a]. Future work may be to look for evidence of this process during our CalNex study and implement such a scheme into GEOS-Chem.

References

Bahreini, R., J. L. Jimenez, J. Wang, R. C. Flagan, J. H. Seinfeld, J. T. Jayne, and D. R. Worsnop (2003), Aircraft-based aerosol size and composition measurements during ACE-Asia using an Aerodyne aerosol mass spectrometer, *J. Geophys. Res.*, *108*, 22 PP., doi:200310.1029/2002JD003226.

Beer, R. et al. (2008), First satellite observations of lower tropospheric ammonia and methanol, *Geophys. Res. Lett.*, *35*(9), doi:10.1029/2008GL033642.

Bishop, G. A., A. M. Peddle, D. H. Stedman, and T. Zhan (2010), On-road emission measurements of reactive nitrogen compounds from three California cities, *Environ. Sci. Technol.*, *44*(9), 3616–3620, doi:10.1021/es903722p.

Bouwman, A. F., D. S. Lee, W. A. H. Asman, F. J. Dentener, K. W. Van Der Hoek, and J. G. J. Olivier (1997), A global high-resolution emission inventory for ammonia, *Global Biogeochem. Cycles*, *11*(4), 561, doi:10.1029/97GB02266.

Chen, D., Y. Wang, M. B. McElroy, K. He, R. M. Yantosca, and P. Le Sager (2009), Regional CO pollution and export in China simulated by the high-resolution nested-grid GEOS-Chem model, *Atmos. Chem. Phys.*, *9*(11), 3825–3839, doi:10.5194/acp-9-3825-2009.

Chow, J. C., J. G. Watson, E. M. Fujita, Z. Lu, D. R. Lawson, and L. L. Ashbaugh (1994), Temporal and spatial variations of PM2.5 and PM10 aerosol in the Southern California air quality study, *Atmos. Environ.*, *28*(12), 2061–2080, doi:10.1016/1352-2310(94)90474-X.

Chow, J. C., J. G. Watson, Z. Lu, D. H. Lowenthal, C. A. Frazier, P. A. Solomon, R. H. Thuillier, and K. Magliano (1996), Descriptive analysis of PM2.5 and PM10 at regionally representative locations during SJVAQS/AUSPEX, *Atmos. Environ.*, *30*(12), 2079–2112, doi:10.1016/1352-2310(95)00402-5.

Chow, J. C., J. G. Watson, D. H. Lowenthal, R. T. Egami, P. A. Solomon, R. H. Thuillier, K. Magliano, and A. Ranzieri (1998), Spatial and temporal variations of particulate precursor gases and photochemical reaction products during SJVAQS/AUSPEX ozone episodes, *Atmos. Environ.*, *32*(16), 2835–2844, doi:10.1016/S1352-2310(97)00449-4.

Chow, J. C., J. G. Watson, L. L. Ashbaugh, and K. L. Magliano (2003), Similarities and differences in PM10 chemical source profiles for geological dust from the San Joaquin Valley, California, *Atmos. Environ.*, *37*(9–10), 1317–1340, doi:10.1016/S1352-2310(02)01021-X.

Chow, J. C., J. G. Watson, D. H. Lowenthal, K. Park, P. Doraiswamy, K. Bowers, and R. Bode (2007), Continuous and filter-based measurements of PM2.5 nitrate and sulfate at the Fresno Supersite, *Environ. Monit. Assess.*, *144*(1-3), 179–189, doi:10.1007/s10661-007-9987-5.

Clarisse, L., C. Clerbaux, F. Dentener, D. Hurtmans, and P.-F. Coheur (2009), Global ammonia distribution derived from infrared satellite observations, *Nature Geosci.*, *2*(7), 479–483, doi:10.1038/ngeo551.

Clarisse, L., M. W. Shephard, F. Dentener, D. Hurtmans, K. Cady-Pereira, F. Karagulian, M. Van Damme, C. Clerbaux, and P.-F. Coheur (2010), Satellite monitoring of ammonia: A case study of the San Joaquin Valley, *J. Geophys. Res.*, *115*(D13), doi:10.1029/2009JD013291.

Dentener, F. J., and P. J. Crutzen (1994), A three-dimensional model of the global ammonia cycle, *J. Atmos. Chem*, *19*(4), 331–369, doi:10.1007/BF00694492.

Ellis, R.A., J. G. Murphy, P. L. Hayes, M. J. Cubison, A. M. Ortega, J. L. Jimenez, J. Liu, R. Weber, P. Veres, A. K. Cochran, and J. M. Roberts, Gas-particle partitioning of ammonia at the CalNex-LA ground site and the influence of aerosol pH, *J. Geophys. Res.*, in preparation.

Engling, G., P. Herckes, S. M. Kreidenweis, W. C. Malm, and J. L. Collett Jr. (2006), Composition of the fine organic aerosol in Yosemite National Park during the 2002 Yosemite Aerosol Characterization Study, *Atmos. Environ.*, *40*(16), 2959–2972, doi:10.1016/j.atmosenv.2005.12.041.

Erisman, J. W., A. Bleeker, J. Galloway, and M. S. Sutton (2007), Reduced nitrogen in ecology and the environment, *Environ. Pollut.*, *150*(1), 140–149, doi:10.1016/j.envpol.2007.06.033.

Erisman, J. W., M. A. Sutton, J. Galloway, Z. Klimont, and W. Winiwarter (2008), How a century of ammonia synthesis changed the world, *Nature Geosci.*, *1*(10), 636–639, doi:10.1038/ngeo325.

Fairlie, T. D., D. J. Jacob, J. E. Dibb, B. Alexander, M. A. Avery, A. van Donkelaar, and L. Zhang (2010), Impact of mineral dust on nitrate, sulfate, and ozone in transpacific Asian pollution plumes, *Atmos. Chem. Phys.*, *10*(8), 3999–4012, doi:10.5194/acp-10-3999-2010.

Farquhar, G. D., P. M. Firth, R. Wetselaar, and B. Weir (1980), On the gaseous exchange of ammonia between leaves and the environment: determination of the ammonia compensation point, *Plant Physiol.*, *66*(4), 710–714, doi:10.1104/pp.66.4.710.

Flechard, C. R., D. Fowler, M. A. Sutton, and J. N. Cape (1999), A dynamic chemical model of bi-directional ammonia exchange between semi-natural vegetation and the atmosphere, *Q. J. Roy. Meteorol. Soc.*, *125*(559), 2611–2641, doi:10.1002/qj.49712555914.

Fountoukis, C., and A. Nenes (2007), ISORROPIA II: a computationally efficient thermodynamic equilibrium model for K+–Ca2+–Mg2+–NH4+–Na+–SO42−–NO3−–Cl−–H2O aerosols, *Atmos. Chem. Phys.*, *7*(17), 4639–4659, doi:10.5194/acp-7-4639-2007.

Goebes, M. D., R. Strader, and C. Davidson (2003), An ammonia emission inventory for fertilizer application in the United States, *Atmos. Environ.*, *37*(18), 2539–2550, doi:10.1016/S1352-2310(03)00129-8.

Hall, J. V., V. Brajer, and F. W. Lurmann (2008), Measuring the gains from improved air quality in the San Joaquin Valley, *J. Environ. Manage.*, *88*(4), 1003–1015, doi:10.1016/j.jenvman.2007.05.002.

Hand, J. L., B. A. Schichtel, M. Pitchford, W. C. Malm, and N. H. Frank (2012), Seasonal composition of remote and urban fine particulate matter in the United States, *J. Geophys. Res.*, *117*(D5), doi:10.1029/2011JD017122.

IPCC (2007), *Climate Change 2007: The Physical Science Basis. Contribution of Working Group I to the Fourth Assessment Report of the Intergovernmental Panel on Climate Change*.

Jacob, D. J., J. W. Munger, J. M. Waldman, and M. R. Hoffmann (1986), The H2SO4-HNO3-NH3 system at high humidities and in fogs 1. spatial and temporal patterns in the San Joaquin Valley of California, *J. Geophys. Res.*, *91*(D1), 1073–1088, doi:10.1029/JD091iD01p01073.

Jayne, J. T., D. C. Leard, X. Zhang, P. Davidovits, K. A. Smith, C. E. Kolb, and D. R. Worsnop (2000), Development of an aerosol mass spectrometer for size and composition analysis of submicron particles, *Aerosol Sci. Tech.*, *33*(1-2), 49–70, doi:10.1080/027868200410840.

Jimenez, J. L. et al. (2003), Ambient aerosol sampling using the Aerodyne Aerosol Mass Spectrometer, *J. Geophys. Res.*, *108*, 13 PP., doi:200310.1029/2001JD001213.

Jordan, C. E., J. E. Dibb, B. E. Anderson, and H. E. Fuelberg (2003), Uptake of nitrate and sulfate on dust aerosols during TRACE-P, *J. Geophys. Res.*, *108*(D21), 8817, doi:10.1029/2002JD003101.

Lefer, B. L., and R. W. Talbot (2001), Summertime measurements of aerosol nitrate and ammonium at a northeastern U.S. site, *J. Geophys. Res.*, *106*(D17), 20365–20378, doi:10.1029/2000JD900693.

Liu, H., D. J. Jacob, I. Bey, and R. M. Yantosca (2001), Constraints from 210Pb and 7Be on wet deposition and transport in a global three-dimensional chemical tracer model driven by assimilated meteorological fields, *J. Geophys. Res.*, *106*(D11), PP. 12,109–12,128, doi:200110.1029/2000JD900839.

Mari, C., D. J. Jacob, and P. Bechtold (2000), Transport and scavenging of soluble gases in a deep convective cloud, *J. Geophys. Res.*, *105*(D17), PP. 22,255–22,267, doi:200010.1029/2000JD900211.

Martinelango, P. K., P. K. Dasgupta, and R. S. Al-Horr (2007), Atmospheric production of oxalic acid/oxalate and nitric acid/nitrate in the Tampa Bay airshed: Parallel pathways, *Atmos. Environ.*, *41*(20), 4258–4269, doi:10.1016/j.atmosenv.2006.05.085.

Murray, L. T., D. J. Jacob, J. A. Logan, R. C. Hudman, and W. Koshak, Optimized regional and interannual variability of lightning in a global chemical transport model constrained by LIS/OTD satellite data, *J. Geophys. Res*, in press.

Myriokefalitakis, S., K. Tsigaridis, N. Mihalopoulos, J. Sciare, A. Nenes, K. Kawamura, A. Segers, and M. Kanakidou (2011), In-cloud oxalate formation in the global troposphere: a 3-D modeling study, *Atmos. Chem. Phys.*, *11*(12), 5761–5782, doi:10.5194/acp-11-5761-2011.

Nemitz, E., C. Milford, and M. A. Sutton (2001), A two-layer canopy compensation point model for describing bi-directional biosphere-atmosphere exchange of ammonia, *Q. J. Roy. Meteorol. Soc.*, *127*(573), 815–833, doi:10.1002/qj.49712757306.

Nenes, A., S. N. Pandis, and C. Pilinis (1998), ISORROPIA: a new thermodynamic equilibrium model for multiphase multicomponent inorganic aerosols, *Aquat. Geochem.*, *4*(1), 123–152, doi:10.1023/A:1009604003981.

Neuman, J. A. et al. (2002), Fast-response airborne in situ measurements of HNO3 during the Texas 2000 Air Quality Study, *J. Geophys. Res.*, *107*, 14 PP., doi:200210.1029/2001JD001437.

Neuman, J. A. et al. (2003), Variability in ammonium nitrate formation and nitric acid depletion with altitude and location over California, *J. Geophys. Res.*, *108*, 12 PP., doi:200310.1029/2003JD003616.

Nowak, J. B., J. A. Neuman, K. Kozai, L. G. Huey, D. J. Tanner, J. S. Holloway, T. B. Ryerson, G. J. Frost, S. A. McKeen, and F. C. Fehsenfeld (2007), A chemical ionization mass spectrometry technique for airborne measurements of ammonia, *J. Geophys. Res.*, *112*(D10), doi:10.1029/2006JD007589.

Nowak, J. B., J. A. Neuman, R. Bahreini, C. A. Brock, A. M. Middlebrook, A. G. Wollny, J. S. Holloway, J. Peischl, T. B. Ryerson, and F. C. Fehsenfeld (2010), Airborne observations of ammonia and ammonium nitrate formation over Houston, Texas, *J. Geophys. Res.*, *115*(D22), doi:10.1029/2010JD014195.

Nowak, J. B., J. A. Neuman, R. Bahreini, A. M. Middlebrook, J. S. Holloway, S. A. McKeen, D. D. Parrish, T. B. Ryerson, and M. Trainer (2012), Ammonia sources in the California South Coast Air Basin and their impact on ammonium nitrate formation, *Geophys. Res. Lett.*, *39*(7), doi:10.1029/2012GL051197.

Park, R. J., D. J. Jacob, B. D. Field, and R. M. Yantosca (2004), Natural and transboundary pollution influences on sulfate-nitrate-ammonium aerosols in the United States: Implications for policy, *J. Geophys. Res.*, *109*(D15), doi:10.1029/2003JD004473.

Pye, H. O. T., H. Liao, S. Wu, L. J. Mickley, D. J. Jacob, D. K. Henze, and J. H. Seinfeld (2009), Effect of changes in climate and emissions on future sulfate-nitrate-ammonium aerosol levels in the United States, *J. Geophys. Res.*, *114*(D1), doi:10.1029/2008JD010701.

Rastigejev, Y., R. Park, M. P. Brenner, and D. J. Jacob (2010), Resolving intercontinental pollution plumes in global models of atmospheric transport, *J. Geophys. Res.*, *115*(D2), doi:10.1029/2009JD012568.

Russell, A. G., and G. R. Cass (1986), Verification of a mathematical model for aerosol nitrate and nitric acid formation and its use for control measure evaluation, *Atmos. Environ.*, *20*(10), 2011–2025, doi:10.1016/0004-6981(86)90342-2.

Ryerson, T. B. et al. (1998), Emissions lifetimes and ozone formation in power plant plumes, *J. Geophys. Res.*, *103*(D17), PP. 22,569–22,583, doi:199810.1029/98JD01620.

Schumann, U., and H. Huntrieser (2007), The global lightning-induced nitrogen oxides source, *Atmos. Chem. Phys.*, *7*(14), 3823–3907, doi:10.5194/acp-7-3823-2007.

Seinfeld, J. H., and S. N. Pandis (2006), *Atmospheric Chemistry and Physics - From Air Pollution to Climate Change (2nd Edition)*, John Wiley & Sons.

State of California (2012), Department of Finance, *Interim Population Projections for California and Its Counties 2010-2050*.

Steiner, A. L., S. Tonse, R. C. Cohen, A. H. Goldstein, and R. A. Harley (2006), Influence of future climate and emissions on regional air quality in California, *J. Geophys. Res.*, *111*(D18), D18303, doi:10.1029/2005JD006935.

Sullivan, R. C., S. A. Guazzotti, D. A. Sodeman, and K. A. Prather (2007), Direct observations of the atmospheric processing of Asian mineral dust, *Atmos. Chem. Phys.*, *7*(5), 1213–1236, doi:10.5194/acp-7-1213-2007.

Sutton, M. A., J. W. Erisman, F. Dentener, and D. Möller (2008), Ammonia in the environment: From ancient times to the present, *Environ. Pollut.*, *156*(3), 583–604, doi:10.1016/j.envpol.2008.03.013.

Trump, M. (2004), The Central Valley of California, with the San Joaquin Valley in the southern sub-region, and the Sacramento Valley in the northern sub-region, *CC BY-SA 3.0* (*http://creativecommons.org/licenses/by-sa/3.0/deed.en*), *http://commons.wikimedia.org/wiki/File:Map_california_central_valley.jpg*.

Vicars, W. C., and J. O. Sickman (2011), Mineral dust transport to the Sierra Nevada, California: Loading rates and potential source areas, *J. Geophys. Res.*, *116*(G1), G01018, doi:10.1029/2010JG001394.

Vitousek, P. M. (1994), Beyond Global Warming: Ecology and Global Change, *Ecology*, *75*(7), 1862–1876, doi:10.2307/1941591.

Wang, Y. X., M. B. McElroy, D. J. Jacob, and R. M. Yantosca (2004), A nested grid formulation for chemical transport over Asia: Applications to CO, *J. Geophys. Res.*, *109*, 20 PP., doi:200410.1029/2004JD005237.

Watson, J. G., J. C. Chow, J. L. Bowen, D. H. Lowenthal, S. Hering, P. Ouchida, and W. Oslund (2000), Air quality measurements from the Fresno Supersite, *J. Air Waste Manag. Assoc.*, *50*(8), 1321–1334.

van der Werf, G. R., D. C. Morton, R. S. DeFries, L. Giglio, J. T. Randerson, G. J. Collatz, and P. S. Kasibhatla (2009), Estimates of fire emissions from an active deforestation region in the southern Amazon based on satellite data and biogeochemical modelling, *Biogeosciences*, *6*(2), 235–249, doi:10.5194/bg-6-235-2009.

Wesely, M. L. (1989), Parameterization of surface resistances to gaseous dry deposition in regional-scale numerical models, *Atmos. Environ.*, *23*(6), 1293–1304, doi:10.1016/0004-6981(89)90153-4.

Wexler, A. S., and S. L. Clegg (2002), Atmospheric aerosol models for systems including the ions H+, NH4+, Na+, SO42−, NO3−, Cl−, Br−, and H2O, *J. Geophys. Res.*, *107*(D14), 4207, doi:10.1029/2001JD000451.

Wiedinmyer, C., S. K. Akagi, R. J. Yokelson, L. K. Emmons, J. A. Al-Saadi, J. J. Orlando, and A. J. Soja (2011), The Fire INventory from NCAR (FINN): a high resolution global model to estimate the emissions from open burning, *Geosci. Model Dev.*, *4*(3), 625–641, doi:10.5194/gmd-4-625-2011.

Zhang, L., L. P. Wright, and W. A. H. Asman (2010a), Bi-directional air-surface exchange of atmospheric ammonia: A review of measurements and a development of a big-leaf model for applications in regional-scale air-quality models, *J. Geophys. Res.*, *115*(D20), doi:10.1029/2009JD013589.

Zhang, L., D. J. Jacob, E. M. Knipping, N. Kumar, J. W. Munger, C. C. Carouge, A. van Donkelaar, Y. X. Wang, and D. Chen (2012), Nitrogen deposition to the United States: distribution, sources, and processes, *Atmos. Chem. Phys.*, *12*(10), 4539–4554, doi:10.5194/acp-12-4539-2012.

Zhang, Y., P. Liu, X.-H. Liu, B. Pun, C. Seigneur, M. Z. Jacobson, and W.-X. Wang (2010b), Fine scale modeling of wintertime aerosol mass, number, and size distributions in central California, *J. Geophys. Res.*, *115*(D15), doi:10.1029/2009JD012950.